Journal Pre-proof

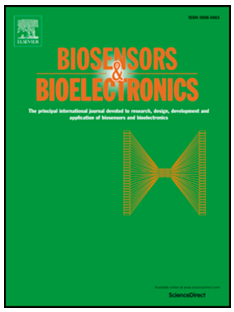

Nanomaterial-based electrochemical sensors and biosensors for the detection of pharmaceutical compounds

Lanting Qian, Sharmila Durairaj, Scott Prins, Aicheng Chen

PII: S0956-5663(20)30822-8

DOI: https://doi.org/10.1016/j.bios.2020.112836

Reference: BIOS 112836

To appear in: *Biosensors and Bioelectronics*

Received Date: 1 June 2020

Revised Date: 16 November 2020

Accepted Date: 20 November 2020

Please cite this article as: Qian, L., Durairaj, S., Prins, S., Chen, A., Nanomaterial-based electrochemical sensors and biosensors for the detection of pharmaceutical compounds, *Biosensors and Bioelectronics* (2020), doi: https://doi.org/10.1016/j.bios.2020.112836.

Credit authorship contribution statement

Lanting Qian: Methodology, Data curation, Formal analysis, Writing - original draft. **Sharmila Durairaj**: Methodology, Formal analysis, Writing - original draft; **Scott Prins**: Investigation, Visualization, Writing - review & editing. **Aicheng Chen**: Conceptualization, Supervision, Funding acquisition, Writing - review & editing.

Nanomaterial-based electrochemical sensors and biosensors for the detection of pharmaceutical compounds

Lanting Qian, Sharmila Durairaj, Scott Prins, Aicheng Chen*

Electrochemical Technology Centre, Department of Chemistry, University of Guelph, 50 Stone Road East, Guelph, Ontario N1G 21, Canada

* Corresponding author. Email: aicheng@uoguelph.ca

Abstract

The surging growth of the pharmaceutical industry is a result of the rapidly increasing human population, which has inevitably led to new biomedical and environmental issues. Aside from the quality control of pharmaceutical production and drug delivery, there is an urgent need for precise, sensitive, portable, and cost-effective technologies to track patient overdosing and to monitor ambient water sources and wastewater for pharmaceutical pollutants. The development of advanced nanomaterial-based electrochemical sensors and biosensors for the detection of pharmaceutical compounds has garnered immense attention due to their advantages, such as high sensitivity and selectivity, real-time monitoring, and ease of use. This review article surveys state-of-the-art nanomaterials-based electrochemical sensors and biosensors for the detection and quantification of six classes of significant pharmaceutical compounds, including anti-inflammatory, anti-depressant, anti-bacterial, anti-viral, anti-fungal, and anti-cancer drugs. Important factors such as sensor/analyte interactions, design rationale, fabrication, characterization, sensitivity, and selectivity are discussed. Strategies for the development of high-performance electrochemical sensors and biosensors tailored toward specific pharmaceuticals are highlighted to provide readers and scientists with an extensive toolbox for the detection of a wide range of pharmaceuticals. Our aims are two-fold: (i) to inspire readers by further elucidating the properties and functionalities of existing nanomaterials for the detection of pharmaceuticals; and (ii) to provide examples of the potential opportunities that these

devices have for the advanced sensing of pharmaceutical compounds toward safeguarding human health and ecosystems on a global scale.

Keywords: electrochemistry; nanomaterials; sensor; biosensor; drug.

1. Introduction

As pharmaceutical industries expand to keep pace with the growth of human populations, the global market for pharmaceutical industries reached $1.25 trillion dollars in 2019 and is projected to attain $1.5 trillion in 2023. To put this into context, there was a 207.9 % increase in pharmaceutical revenues from 2005 to 2019. Consequently, two major issues have emerged: (i) many pharmaceuticals are misused/abused; thus, cheap, portable, and accurate sensors are required for various applications, such as the tracking of drug overdoses, or for biomedical monitoring applications; and (ii) the need to monitor and track pharmaceutical contaminants in ambient water sources for the protection of human and ecological health.

Drug overdose in many countries has become more serious than ever due to inadequate regulations. For instance, the National Center for Health Statistics reported 69,029 deaths as the result of overdosing non-steroidal anti-inflammatory drugs from February 2018 to February 2019, which translated to a 5.5% increase from 2017 to 2018 (Hall et al., 2008; National Center for Health Statistics, 2017). The National Center for Health Statistics in the US reported a spike in anti-depressant overdoses in 2017 with more than 5000 deaths compared to 3889 in 2010 (National Center for Health Statistics, 2017). The fatalities from overdosing anti-depressants had, on average, increased around 6% per year from 2005 to 2018. Germany's Ministry for the Environment reported that a total of 203 pharmaceuticals with significant concentrations were detected in the ambient aquatic systems of 71 countries, which included a majority of analgesics, antibiotics, as well as anti-inflammatory and anti-

fungal drugs Japanese health authorities conducted national testing for antibiotics in 37 rivers, and their combined concentration was as high as 626 ng L^{-1} (Hall et al., 2008). Advanced analytical techniques such as GC-MS, LC-MS/MS, UPLC, and HPLC have been commonly employed for the quantification of pharmaceutical drugs (Maduraiveeran et al., 2018; Nováková et al., 2006; Wolfender, 2009). However, these techniques are limited due to their high cost and limited portability. Therefore, electrochemical techniques are attractive alternatives in contrast to the aforementioned techniques.

The incorporation of nanomaterials has had a great impact on the development of electrochemical sensors. Significant progress has been made toward the synthesis of nanomaterials with controllable morphologies, dimensions, surface charges, and physicochemical properties (Paulchamy et al., 2015; Boles et al., 2016; Chen and Chatterjee, 2013; Duan et al., 2015; Sun and Xia, 2002). Consequently, the attributes of selected nanomaterials can be tailored to specific analytes for electrochemical sensing. A comprehensive elucidation of the physicochemical and electronic interactions that occur at the interfaces between nanomaterial-based electrodes and analytes of interest are critical for exploiting the full potential of advanced electrochemical sensors. Scheme 1 lists various nanomaterials which have been extensively investigated and incorporated in the design of electrochemical sensors and biosensors for the detection of six classes of important pharmaceutical compounds, including anti-inflammatory, anti-depressant, anti-bacterial, anti-viral, anti-fungal, and anti-cancer drugs. This review aims to survey the state-of-the-art nanomaterial-based electrochemical sensing with the capacity to address the aforementioned challenges in response to the surge in pharmaceutical industries. Through the exploration of numerous nanomaterials and their properties for the detection of specific pharmaceuticals in consideration of their interactivity, this review will endeavour to provide new insights toward the development of more efficient and customizable electrochemical sensors.

2. Electrochemical methods

Electrochemical detection occurs at the interface between an analyte of interest and the working electrode to which a potential is applied with respect to the reference electrode, while the corresponding current is measured. Notably, there are numerous electroanalytical methods that can be utilized for the electrochemical detection of pharmaceuticals. Certain techniques may be more suitable for the detection of pharmaceutical compounds based on specific electrochemical interfaces between the nanomaterials employed, the analytes of interest, and the intended application. Common electrochemical strategies may be classified as voltammetry, amperometry, potentiometry, and electrochemical impedance spectroscopy (EIS) (Bard and Faulkner, 2001).

Notably, voltammetric techniques are the most commonly employed, which are discussed more thoroughly here. Cyclic voltammetry (CV) has emerged as the predominant characterization method for the initial study of analytes. This technique is based on varying the applied potential of the working electrode in both the forward (anodic sweep) and the reverse (cathodic sweep) directions, while measuring the corresponding current. CV is useful for determining the reaction kinetics, which include the number of electrons transferred, stoichiometry, reversibility, and the type of reaction (Bard and Faulkner, 2001; Elgrishi et al., 2018). This technique is also useful for determining the diffusion coefficient, charge transfer coefficient, and activation barrier, which helps to elucidate the reaction kinetics of the system under study. Pulse techniques such as normal pulse voltammetry (NPV), differential pulse voltammetry (DPV), and square wave voltammetry (SWV) are more commonly used for electrochemical detection due to their increased sensitivity compared to CV. These pulse techniques greatly improve the signal of the Faradaic response relative to the response generated by the capacitive current. This is achieved by taking advantage of the fact that the capacitive current decays much faster than the Faradaic response, often within 1 or 2 milliseconds. Following the decay of the

capacitive current, the Faradaic response under transport limited linear diffusion conditions is modelled by the Cottrell equation, such that the Faradaic current is inversely proportional to time (Compton and Banks, 2007). DPV is typically capable of achieving detection limits of 10^{-8} M or lower.

Both NPV and DPV employ a series of potential pulses; however, DPV differs in that rather than gradually increasing the amplitude of the pulse as in NPV, the pulse amplitude is fixed and superimposed on a gradually increasing potential staircase. The current is measured just before the application of each pulse and at the end of each pulse. For these pulse techniques, the parameters, in particular the pulse width and amplitude, are important to optimize the signal response. The amplitude of each pulse is generally between 20 to 80 mV, whereas the width may be varied from 0.02 to 0.1 s (Scholz, 2015). The optimization of the pulse amplitude and width is highly dependent on the material being employed. A sensing substrate with high capacitance may have its capacitive current decay at a much slower rate; therefore, decreasing the amplitude to eliminate the large capacitive current, or increasing the pulse width may be chosen to achieve more sensitive detection (Monk, 2002). Specifically, for sensing platforms with high surface areas, although there may be more oxidation/reduction events occurring at the surface, the capacitive current may overshadow any Faradaic current as it decays at a slow rate. This issue may be addressed by using a lower pulse amplitude; however, this could also decrease the Faradaic response.

Another predominant electrochemical technique for sensing applications is SWV. As the name suggests, this technique employs a square wave that is superimposed on a potential staircase, similarly to DPV. The square wave pulse is comprised of a forward and reverse pulse, and the difference is obtained by subtracting the forward and reverse currents, which is then plotted against the staircase potential as the final result of the measurements (Chen and Shah, 2013). The advantage of SWV in contrast to DPV is the cancellation of capacitive contributions when subtracting the forward pulse from

the reverse pulse, resulting in more sensitive detection limits. SWV is also useful for elucidating the electrode kinetics for many reactions by employing a rapid scan rate (~1V s^{-1}) and a rapid data collection speed combined with computer processing (Bard and Faulkner, 2001; Chen and Shah, 2013; Scholz, 2015). However, there are some limitations to this technique due to its fast scan rate; SWV is better suited for the analysis of reversible and rapid electrode processes and those coupled with fast chemical reactions than studying quasi-reversible reactions with slow electrode kinetics. In some cases, if the material possesses a high capacitive current, it may also result in broader Faradaic response peaks.

Amperometric sensors are based on the current measurement at an applied electrode potential; they exhibit some notable advantages such as a low detection limit and high selectivity in comparison to the voltammetry-based electrochemical sensors (Yashin et al., 2004). Enzyme-based amperometric sensors have been widely explored because of their high sensitivity and selectivity; they can operate with small sample volumes of complex matrices (Rocchitta et al., 2016). However, one of the main challenges of the enzymatic electrochemical sensing is the stability, which may be caused by the denature of enzymes or the fouling from the species present in the sample matrix or formed during the sensing process. To summarize, employing specific electrochemical methods that are best suited for the sensor and analytes of interest is essential to fully realize the potential of the developed electrochemical sensors and biosensors.

3. Development of nanomaterials for electrochemical sensing

The incorporation of nanomaterials has enabled novel and effective sensing platforms to be developed. This section covers several important types of nanomaterials and nanocomposites, which have been widely employed for the design of high-performance electrochemical sensors and biosensors for the detection of pharmaceutical compounds.

3.1 Carbon-based nanomaterials

Carbon-based nanomaterials offer several unique advantages in comparison to many other nanomaterials. They exhibit high surface-to-volume ratios, high electrical conductivity, long-term chemical stability, and enhanced mechanical strength (Adhikari et al., 2015). These characteristics enable carbon-based nanomaterials to have lower detection limits and higher sensitivities (Baptista et al., 2015; Power et al., 2018; Rao et al., 2009; Yang et al., 2015). In many cases they can also be employed as substrates for surface functionalization via aptamers, enzymes, and various nanomaterials.

3.1.1 Carbon nanotubes: Carbon nanotubes (CNTs) have become increasingly popular for the creation of advanced electrochemical sensors due to their excellent conductivity and high tunability (e.g., length and diameter). Depending on the specific molecular structure and chemical composition of pharmaceuticals, CNTs may be used to promote electron transfer of many reactions and facilitate adsorption of organic molecules (Bakshi et al., 2010; Camilli and Passacantando, 2018; Pumera, 2009). CNTs can also be used as substrates for further functionalization, which due to their excellent conductivity and high surface-to-volume ratio tends to increase the performance of catalysts on the surface. Moreover, CNTs may produce synergetic effects that promote sensing (Espinosa et al., 2007; Jung et al., 2015; Mallakpour and Khadem, 2016). Single-walled carbon nanotubes (SWCNTs) consist of a single graphene sheets wrapped into cylindrical tubes with diameters of between 0.4 – 2.5 nm. Apart from their high electrical conductivity, their diminutive size and dimensionality can enhance the electron transfer kinetics in many reactions; furthermore, their high surface-to-volume ratios may greatly improve signal-to-noise ratios in many cases. It is important to note that the dimensions of the nanotubes can be tuned to optimize for the reaction of interest. For instance, Bandyopadhyay et al. reported that by tuning the sizes of single-walled

carbon nanotubes, they were able to successfully intercalate or trap hazardous insecticides, which efficiently promoted the electrochemical oxidation of the molecules (Bandyopadhyay et al., 2017). Multi-walled carbon nanotubes (MWCNTs) are comprised of multiple nested graphene sheet layers that have variable diameters up to 100 nm. Similar to SWCNTs, MWCNTs also exhibit high surface-area to volumes, excellent conductivity, and are highly tunable. However, there are also striking differences between SWCNTs and MWCNTs, which are important to consider when designing electrochemical sensors (Duclaux, 2002). SWCNTs are generally more flexible, whereas MWCNTs are rather rigid. In addition, the production of SWCNT requires a catalyst and are generally more expensive.

3.1.2 Graphene and graphene oxide: Graphene is composed of a single layer of sp^2-hybridized carbon arranged in a hexagonal lattice, which exhibits unique electronic and structural attributes that are useful for sensing platforms (Basu and Bhattacharyya, 2012; Donarelli and Ottaviano, 2018; Zhou et al., 2009). Graphene oxide (GO) contains oxygen functional groups that can be tailored to optimize electrochemical sensing for specific analytes; however, the presence of the oxygen functional groups greatly reduces the surface conductivity (Lu et al., 2016). Notably, these oxygen functional groups can be reduced chemically, electrochemically or thermally, which may introduce monovacancy or multi-vacancy defects. Studies have shown that the presence of these defects can significantly promote the catalysis of many organic molecules (Su and Loh, 2013; Sun et al., 2012). Further, doping with heteroatoms can induce surface charges, which can be useful for sensing in cases where electrostatic interactions occur, in that heteroatoms may serve as catalytic centers for various molecules (Kong et al., 2014). Similar to CNTs, graphene-based nanomaterials may also be used as substrates for further functionalization. Moreover, graphene and GO materials can stabilize

deposited nanoparticles (NPs), while preventing their agglomeration (Ravat et al., 2016; Wu et al., 2013).

3.2 Noble metal nanomaterials

Metal nanoparticles are commonly utilized for the detection of pharmaceutical analytes because of their impressive catalytic abilities due to their sizes and shapes. The growth of nanoparticles from seeds into their resulting nanostructures is a result of the physical and chemical properties of the metal and its interactions with the surrounding environment. The sizes, shapes, and facets of the nanoparticles can be controlled through the careful design of their surfaces and localized environments through the use of capping agents and supramolecular interactions, which play a significant role in the formation of nanoparticles (Bell, 2003; Heiligtag and Niederberger, 2013; Sun and Zeng, 2002; Suryanarayana, 2005; Verma et al., 2014). The selection of nanoparticles for a specific analyte is based on the size, adsorption strength, orientation, and chemical composition of the compound. The synergistic effects of bimetallic or trimetallic nanoparticles can also be employed to promote catalytic sensing. Macrocyclic compounds have found use in nanomaterial synthesis as they have the capacity to accommodate tailored guest-host interactions due to their altering hydrophobicity and hydrophilicity at specific locations of the macrocycle. Examples include either the interior or exterior of the cyclodextrin rings, or at the edge sites of the cucurbiturils bands (Dumestre et al., 2004). Various three-dimensional (3D) nanomaterials such as those with hollow interiors, nanopores, hollow cubes and spheres may be employed as sensing platforms (Jia et al., 2008; Lahav et al., 2003; Mohanty, 2011; White et al., 2009). In some cases, bimetallic and trimetallic alloys are synthesized to enhance sensing abilities as the alloys may exhibit synergetic effects. The origin of the synergetic effects between different metals may be attributed to the stabilization of intermediates, enhancement of the adsorption of analytes, proton

transfer, and lowering of the activation barrier of the reactions between analytes and the alloy (Bracey et al., 2009; Z. Liu et al., 2016; Long et al., 2015; Mailu et al., 2010; Moghimi et al., 2015; Nguyen et al., 2016; Sankar et al., 2012). One of the major advantages of metal-based nanomaterials compared to carbon-based nanomaterials is that they are generally more selective to the analytes being examined; the interactions between the metal nanomaterials and the targeted molecules are tunable by changing their morphology, structure and composition.

3.3 Carbon-metal nanocomposites

Metal-carbon nanocomposites have been widely explored for sensing applications due to their high conductivity, extensive surface area, and relative cost effectiveness. The large surface areas of carbon nanomaterials can host and stabilize nanoparticles, while increasing the population of reactive sites. Metal oxides and metal nanoparticles are often synthesized by combining graphene-based materials. Specifically, in the case of graphene/GO-metal nanoparticles nanocomposites, GO can stabilize the nanoparticles and minimize their aggregation.

3.4 TiO_2-supported nanomaterials

TiO_2-supported nanomaterials are commonly employed for electrochemical sensing due to their chemical stability, biocompatibility, unique photo-catalytic properties, and multi-functionality. Using TiO_2 as a support may take advantage of the known properties of other materials, such as when TiO_2 nanorods or tubes are decorated with noble-metal nanoparticles. The nanoparticles are more active than the TiO_2 support material, which assists with conductivity/charge transfer to decrease the probability of back-reactions and the recombination of charge carriers. An added benefit is that Ti is a biocompatible material, which makes it particularly suitable for biomedical applications. It is also a naturally abundant material, which makes the cost of producing materials from Ti lower than

those comprised of noble metals. Moreover, TiO_2 allows for harsher conditions during the synthesis and operation of the nanomaterial and the electrochemical sensor (Bai and Zhou, 2014; Chen and Mao, 2007).

3.5 Conductive polymers

Over the last decade, conductive polymers have been incorporated into synthetic composites for sensing applications. Conductive polymers are attractive due to their unique behaviour upon exposure to electric fields, their electroactive properties, and most importantly their conductivity (Uzun and Turner, 2016). Generally, these polymers are organic molecules such as polypyrenes, polypyrrole, and polystyrene ethylenedioxythiopene (PEDOT) (Wackerlig and Lieberzeit, 2015). The advantage of utilizing conductive polymers in the fabrication of sensors is to increase their selectivity and sensitivity for targeted analytes. Recently, molecularly imprinted polymer (MIP) composites have gained popularity due to their capacity for enabling the specific design of interactions between the sensing interface and the analyte, which is particularly useful for the detection of analytes in complex biological matrices, where selectivity and fouling are major issues (Alqarni et al., 2020; Y. C. Wong et al., 2020). In addition, MIP offers more stability and reusability in contrast to biological receptors, as generally, it is much lower in cost in comparison to biological transducers. Furthermore, MIP can serve as signal transducers by binding to target molecules, which may induce changes in mass, absorbance, refractive index, conductivity, electric fields, and current. Often the design of MIP can be aided with computational approaches for screening to elucidate potential MIP/analyte interactions. Moreover, the combination of MIP with carbon or metal materials may further increase the performance of the developed electrochemical sensors.

4. Electrochemical sensors and biosensors for drug detection

Electrochemical sensors have been designed and fabricated for the recognition of many types of important drugs which, based on the drug structures, often demand specific sensor interfaces to realize their full detection potential. Novel electrochemical sensors are continually being proposed to augment their sensitivity and stability and to lower the limits of detection. Here we summarize the recent advances of the electrochemical sensing of a number of significant pharmaceutical compounds, which may be classified into six categories based on their functions and medical applications: anti-inflammatory, anti-depressant, anti-bacterial, anti-fungal, anti-viral, and anti-cancer.

4.1 Anti-inflammatory drugs

Nonsteroidal anti-inflammatory drugs (NSAIDs) are used to reduce pain, inflammation, and to decrease fever. Analgesics are akin to NSAIDs as they both treat pain and fever; however, analgesics such as acetaminophen have limited anti-inflammatory activity. Since most NSAIDs are over-the-counter medications, they are one of the most commonly abused drugs. Due to their extensive use by consumers, NSAIDs have caused significant water contamination problems (Lapworth et al., 2012). NSAIDs can be divided into groups based on their chemical structures with the majority being propionic acids (naproxen, ibuprofen), followed by acetylated salicylates (aspirin), acetic acids (diclofenac, indomethacin), and the less common COX-2 inhibitors (celecoxib). The mechanism of action for all NSAIDs is the inhibition of the activity of cyclooxygenase (COX-1 or COX-2) as these enzymes are engaged in the synthesis of prostaglandins, which are involved in the inflammation signalling process (Vane and Botting, 1998).

***4.1.1 Naproxen*:** Being two of the most commonly used NSAIDs, ibuprofen and naproxen are propanoic acid derivatives that contain one and two benzene rings in their chemical structures, respectively. The electrochemical oxidation mechanism of isoniazid and naproxen are very similar: generally, a one electron transfer, which results in the decarboxylation reaction, is followed by an

immediate oxidation to generate an alcohol derivative as the product (He et al., 2018; Stefano et al., 2014). Qian et al. investigated GO and its derivatives and explored the effects of heteroatom doping and the amount of oxygen content on the electrochemical oxidation of naproxen (Qian et al., 2020). It was found that as the oxygen content increased, specifically the epoxy and hydroxyl content on the graphene sheet, the catalytic oxidation of naproxen became stronger. Fig. 1A displays a typical SEM image of GO that consisted of a folded and crumbled structure with irregular edges and rough surfaces. To investigate their electrochemical behaviors, cyclic voltammograms of the synthesized GO and its derivatives were recorded in 5 mM $K_3[Fe(CN)_6]$. As expected, the increased oxygen content decreased the signal of the ferricyanide response and increased the peak separation (Fig. 1B). However, it was determined that GO, which had the highest oxygen content, demonstrated the highest performance toward the electrochemical oxidation of naproxen. Fig. 1C shows a series of the DPV curves as the analyte concentration increased, with the corresponding calibration curve plotted in Fig. 1D. The developed GO sensor, which demonstrated a good limit of detection (LOD) of 1.94 µM and a wide linear range of 10 µM to 1 mM, was verified to successfully detect pharmaceutical tablets with >90 % recovery. Amperometric and potentiometric sensors were developed using nano-spinel zinc ferrite films ($ZnFe_2O_4$) for the detection of naproxen (Kanagasabapathy, 2015). The anodic character of the n-type $ZnFe_2O_4$ (band gap ~ 2 eV) tended to promote the oxidation of organic molecules, while remaining highly tunable. The sensor showed satisfactory sensitivity and LOD of 0.129 µA μM^{-1} and 13 µM, respectively. Furthermore, carbon nanomaterials and metal nanoparticles functionalized with organic polysaccharides such as cyclodextrin or chitosan can be attractive for achieving high sensitivity while retaining excellent selectivity. This was demonstrated by a disposable electrochemical sensor based on a digital disc chip comprised of gold and modified by GO decorated with silver nanoparticles and β-cyclodextrin (AgNPs@GO-β-CD) (Tarahomi et al., 2019). The

developed electrodes were successfully applied for the detection of naproxen tablets and naproxen in human urine samples with good performance, showing their practical value and potential for commercial applications.

Enzymatic electrochemical sensors are often preferred for the detection of biological species such as proteins and metabolites, as they are highly selective, and their functional roles are well documented. The combination of nanomaterials with enzymes of interest not only stabilizes the enzymes but may further improve sensor responses. Rossi et al. reported an amperometric biosensor that employed a cytochrome P450-based electrochemical sensor for the detection of naproxen, which involved the drop-casting of MWCNT and microsomal P4501A2 (msCYP1A2) on a graphite screen-printed electrode (SPE) (Baj-Rossi et al., 2014). This electrochemical sensor exhibited a slightly improved LOD compared to other detection methods and was proved to be successful for monitoring drug delivery, which was investigated using a commercial micro-osmotic pump.

***4.1.2 Ibuprofen*:** Roushani et al. reported an ultrasensitive electrochemical sensor for the detection of ibuprofen, for which an aptamer was covalently attached to electrochemically deposited gold NPs on a glassy carbon electrode (GCE) surface (Roushani and Shahdost-Fard, 2015). An unprecedented LOD of 0.5 pM was yielded with a linear range from 0.005 to 7 nM. The deposition of Au NPs facilitated the oxidation of ibuprofen and increased the active surface area. The aptamer, which enhanced the signal-to-noise ratio of the analyte response and increased the sensitivity, also improved the selectivity of the sensor. In this strategy, an ibuprofen specific aptamer (ssDNA2) hybrid was covalently attached to the AuNP/GCE surface using cysteamine, via the formation of a stable self-assembled monolayer (SAM), and terephthalate as the linking agent (Roushani and Shahdost-Fard, 2015). The sensor fabrication process is illustrated in Fig. 2A, where the AuNPs deposited on the GCE were functionalized with cysteine to form stable SAMs. This was followed by attaching terephthalate and

adding a 3'-amine-terminated capture probe (ssDNA1). Finally, the ssDNA2 was dropped and incubated on the surface of the ssDNA1/terephthalate/Cyst/AuNPs/GCE to form the hybrid sensor. Fig. 2B depicts the DPV responses of the nanoaptasensor to 0.005, 0.01, 0.065, 0.115, 2.0, 4.5, 5.5, 6.5 and 7.0 nM of ibuprofen recorded record in $[Fe(CN)_6]^{3-/4-}$ as the electrolyte solution. It can be seen that as the concentration of analyte increased, the current decreased due to ibuprofen/Apt complex crowding of the electrode surface, which hindered the electron transfer with the redox agent. Fig. 2C shows that the calibration curve ranged from 2 to 7 nM with a LOD of 0.5 pM. For naproxen, Nair et al. also developed a polymer-wrapped AgNP-decorated acid functionalized GO electrochemical sensor, which demonstrated improved sensitivity and a lower LOD compared to a GO only sensor (Nair and Sooraj, 2020).

***4.1.3 Aspirin*:** Aspirin is an acetylated salicylate, similar to propionic acids (naproxen and ibuprofen), contains a carboxylic group and a benzene ring. The oxidation of aspirin involves a two-electron and two-proton transfer process, in which aspirin initially undergoes hydrolysis to yield salicylic acid, followed by the loss of one electron to yield a free radical. Finally, the radical, accompanied by the loss of another electron, rearranges into the final product, 2, 5-dihydrioxybenzoic acid (Kruanetr et al., 2014). Ghadimi et al. reported a poly 4-vinylpyridine (P4VP) wrapped around MWCNT that was drop-cast on a GCE surface. The incorporation of conductive polymers was confirmed to improve the conductivity, electron transfer kinetics, and electrocatalytic activity of the catalyst (Ghadimi et al., 2016). Further, the P4VP served as a stabilizing agent as it wrapped around the MWCNT, which also facilitated their solubility in water and ethanol. The developed electrochemical sensor was successfully applied for the determination of aspirin in formulation tablets which had, on average, over 98 % recovery. The most significant feature of the sensor was that it achieved a very low LOD (4.42 nM) for the detection of aspirin.

The decoration of functionalized groups, self-assembling film, aptamers, and nanomaterials on carbon or metal substrates is a promising approach for the design of electrochemical sensors and biosensors to improve the limit of detection and sensitivity. Diouf et al. reported an electrochemical sensor that was fabricated by self-assembling chitosan capped with AuNPs on a screen-printed carbon electrode (SPCE) (Diouf et al., 2020). While chitosan was proven to have excellent catalytic activity for aspirin, it was electrically insulating. This was addressed through the incorporation of AuNPs to enhance conductivity and promote catalytical activity. AuNPs are widely employed as a sensing element for further modification due to their high surface area-to-volume ratio, high conductivity, and notable catalytic abilities. This prepared sensor achieved a LOD of 0.03 ng L^{-1} via DPV (Diouf et al., 2020).

***4.1.4 Dicolofenac and Celecoxib*:** Dicolofenac and indomethacin belong to the group of NSAID acetic acid derivatives, although they are less common than naproxen, ibuprofen and aspirin for safety reasons. Chethana et al. reported a tyrosine modified carbon paste electrode (CPE) for the detection of diclofenac. Mixing carbon paste with tyrosine greatly increased the sensitivity of the CPE. The developed sensor exhibited a satisfactory LOD of 3.28 µM and a sensitivity of 0.1905 µA μM^{-1}(Chethana et al., 2012). Sataraddi et al. reported the electrochemical detection of indomethacin using an MWCNT modified GCE, which was successfully employed for the determination of a commercial pharmaceutical dosage and the detection of diclofenac in complex human biological fluids (Sataraddi et al., 2014). The electrochemical oxidation of dicolofenac involves a one-electron exchange irreversible oxidation process that breaks up the dicolofenac molecule through the nitrogen atom, generating the fragments 2,6 dichloroaniline and 2-(2-hydroxyprop-2-enyl)phenol. Celecoxib is a less common NSAID; it reduces inflammation by inhibiting the enzyme, COX-2, which is the enzyme responsible for invoking inflammation responses. Arkan et al. described a graphene-gold nanocomposite carbon ionic liquid electrode for the determination of Celecoxib (Arkan et al., 2013).

Graphene and gold nanoparticles exhibited a synergetic effect that improved the performance of the electrochemical sensor.

4.2 Anti-depressants

Anti-depressants are becoming one of the most used, and perhaps abused drugs in the world. The three types of monoamines, which are dopamine, norepinephrine, and serotonin, function as neurotransmitters that transmit signals to the nerve receptors of the brain (Fasipe, 2018). Anti-depressants act by increasing the effects of these neurotransmitters for individuals with depression or mood disorders. While there are five classes of anti-depressants, the most common class is the selective serotonin reuptake inhibitors (SSRIs) that work by preventing the reuptake of serotonin. Fluoxetine (Prozac), Paxil (paroxetine) and sertraline (Zoloft) are the most common ones, which are typically larger in size; thus, they make the electrochemical oxidation more difficult. This is why there are fewer electrochemical sensors developed for these types of drugs in contrast to NSAIDs and other classes of drugs.

4.2.1 Fluoxetine: Alizadeh et al. reported on MIP NPs with highly selective recognition sites for fluoxetine (synthesized by precipitation polymerization), which was then incorporated into a CPE (Alizadeh and Azizi, 2016). The addition of graphene to the synthesized electrode served to enhance sensitivity. Methacrylic acid and vinyl benzene (VB) are required to create the fluoxetine-imprinted polymer as the former provides hydrogen bonding interactions with fluoxetine via its secondary amine and fluorine centers, while the latter participates in the self-assembly of the complex. Fig. 3A shows the optimized conformation of the self-assembled complex, fluoxetine, and the MAA and VB monomers, which was supported by DFT calculations. The effect of incorporating graphene to increase conductivity was compared by examining different integration methods, which are compared in Fig. 3B. Two methods were used for the incorporation of graphene with the nano-MIP-modified

carbon paste electrodes. In the first method, graphene was mixed with graphite and MIP powder (nano-MIP/G_1-CP), whereas the second method involved mixing graphene and a synthesized polymer in dimethyl formamide (nano-MIP/G_2-CP). The optimal results were obtained by nano-MIP/G_2-CP as seen from Fig. 3B. The electrode revealed a LOD of 2.8 nM, while exhibiting excellent sensitivity. A carbon nanofiber-epoxy composite electrode was developed by Ardelean et al. for the simultaneous electrochemical detection of tetracycline and fluoxetine in water; the LOD was reported to be 0.385 μM with a sensitivity of 10.622 μA μM^{-1} (Ardelean et al., 2017).

4.2.2 Paroxetine: Another SSRI, paroxetine, under the brand name Paxil, is often preferred over other SSRIs to treat severe anxiety disorders (Fasipe, 2018). Oghli et al. described a polyoxometalate/reduced graphene oxide (rGO) modified pencil graphite sensor for the trace detection of paroxetine (Oghli and Soleymanpour, 2020). The advantage of pencil graphite electrodes (PGEs) over other carbon-based electrodes was derived from their low cost, high mechanical stability, low background current, and a wide potential window. However, the most significant advantage was the capacity for the removal of memory effects and adsorbed species that caused the electrode fouling, which could be achieved by removing several millimeters of the graphite electrode surface. Phosphotungstic acid, which facilitates proton transfer, was combined with rGO and used as a modifier for the PGE. The developed electrochemical sensor proved to be viable for the analysis of paroxetine in urine and serum with excellent performance. The number of electrons participating in the oxidation of paroxetine was determined to be one, and the charge transfer coefficient was estimated to be 0.34.

4.2.3 Sertraline: Sertraline, sold under the brand name Zoloft, is another popular SSRI. A graphene nanosheet that incorporated MIP as an SPCE was fabricated for sertraline and demonstrated high activity for its detection (Khosrokhavar et al., 2020). A novel Ni-levodopa film was deposited on AuNPs that were bound to enriched MWCNT as the electrocatalyst for the detection of sertraline.

Synergies between the AuNPs and MWCNT at the modified GCE provided a large surface area to allow more Ni(II)-LD complexes to be electropolymerized, which promoted the electrochemical oxidation of sertraline (Shoja et al., 2016), where the use of Ni(II)-Ni(III) redox couples and levodopa was confirmed to have excellent catalytic activity for the oxidation of organic functional groups such as amine, carboxylic, and alcohol groups. The electrochemical oxidation of sertraline involves a two-electron and two-proton process, which was confirmed by the measurements of the peak dependence with respect to the pH change.

4.2.4 **Venlafaxine:** An additional common class of anti-depressants include serotonin and norepinephrine reuptake inhibitors (SNRIs). In contrast to the SSRIs, SNRIs are more aggressive; thus, they are used to treat more severe depression (Fasipe, 2018). Metal oxides, specifically iron oxide (Fe_3O_4), has gained popularity as an attractive electrocatalyst for the oxidation of various organic molecules and sensing of biological species (Li et al., 2011; Li et al., 2015; Sharafeldin et al., 2017; Teymourian et al., 2013). Khalilzadeh et al. reported an electrochemical sensor based on iron oxide nanoparticles deposited on a cellulose nanocrystal-copper nanocomposite (Fe_3O_4@CNC/Cu) for the detection of venlafaxine (Khalilzadeh et al., 2020). Notably, this electrocatalyst was prepared via a plant extract (*Petasites hybridus* leaf), which acted as a stabilizing and reducing agent for copper. This process has been shown to be environmentally compatible (Khalilzadeh et al., 2020). The formed Fe_3O_4@CNC/Cu electrocatalyst was characterized by high resolution TEM, shown in Figs. 4A, B. The developed electrochemical sensor employed DPV for the quantitative analysis of venlafaxine in water samples, with the DPV curves shown in Fig. 4C. The developed electrochemical sensor showed a lower detection limit than those previously reported in literature with a satisfactory sensitivity and linear range.

***4.2.5* TCAs:** Tricyclic anti-depressants (TCAs), being some of the first prescribed anti-depressants in the 1950's, remain a popular choice even today (Kerr et al., 2001). Their structure is composed of three variably sized conjoined rings that incorporate a nitrogen atom in the central ring. Similarly, TCAs function by blocking the reuptake of serotonin, norepinephrine, and acetylcholine at neuroreceptors. Common TCAs include doxepin (Sinequan), imipramine (Tofranil), desipramine (Norpramin), and amoxapine (amoxapine) (Kerr et al., 2001). Jankowska-Sliwinska et al. developed a DNA-based electrochemical sensor for imipramine. Gold paste electrochemical sensors were modified via thiol labelled oligonucleotide sequences and their complementary strands. Interestingly, the DNA modified sensor exhibited higher performance compared to bare gold paste and DNA electrodes (Jankowska-Sliwińska et al., 2015). A bismuth oxide nanotile decorated exfoliated graphite electrode was synthesized via a facile one-pot sono-chemical synthesis, demonstrating a good linear range (0.02 – 82.3 µM) and an acceptable LOD (6 nM) for the detection of imipramine (Yamuna et al., 2020). While glassy carbon and SPEs demonstrated good activities toward desipramine in biological matrices (Knihnicki et al., 2013), a palladium nanoparticle-decorated rGO electrochemical sensor demonstrated improved performance for the detection of imipramine in human urine (Cincotto et al., 2017). Sanghavi et al. employed a titanium dioxide and Amberlite XAD-2 modified glassy CPE for the simultaneous detection of imipramine, trimipramine, and desipramine based on adsorptive stripping voltammetry (Sanghavi and Srivastava, 2013).

4.3 Anti-bacterial drugs

Anti-bacterial drugs (anti-biotics) are widely employed to fight bacterial infections in human, animals, and plants. These drugs are extensively used based on the prevention and cure of the invasion of bacteria through various mechanisms. Their mechanism of action primarily follows four different pathways that include the inhibition or regulation of enzymes present in cell wall synthesis,

nucleic acid metabolism, protein synthesis, and cell membrane disruption. As anti-biotics have provided revolutionary solutions as a remedy for a broad spectrum of infectious diseases from blisters to tuberculosis, the production of antibiotics and their irresponsible use have increased. Due to excessive anti-biotics in all types of environments, bacteria have developed resistance against these drugs. These antibiotic-resistant bacterial strains upsurge the risk of vital infection, which leads to increased dosages for patients. Overdoses can trigger many toxic effects such as allergies, bone marrow toxicity, carcinogenicity, immunopathological effects, nephropathy, hepatoxicity, and reproductive disorders. For the safe monitoring of these drugs in order to minimize the negative impacts on the environment and general human health, improved approaches based on new technologies and materials must be implemented. These drugs can be classified according to their chemical structures and mainly include β-lactam (penicillin), tetracycline (oxytetracycline), sulphonamide (sulfamethizole), fluoroquinolones (ciprofloxacin), and macrolides (erythromycin). The electrochemical detection of some of these critical antibiotics are discussed below.

***4.3.1 Penicillin*:** Penicillin is the most used anti-biotic against staphylococci and streptococci bacterial infections. An electrochemical detection mechanism based on the oxidation of penicillin to penicilloic acid, with the release of carbon dioxide in the presence of penicillinase enzyme combined electrochemical transducer with Pt/Au/L-cysteine nanowire array is displayed in Fig. 5, revealing that the enzymes immobilized on the hybrid Pt-nanowire/Au-NP arrays exhibited high sensitivity for the detection of penicillin and tetracycline. (Li et al., 2019). Penicillins can be differentiated into five varieties: oxacillin, penicillin V, penicillin G, ampicillin, and amoxicillin. Most electrochemical detection techniques were able to analyze one or two types of penicillin (Li et al., 2015). Interestingly, Feier and co-workers investigated the electrochemical behaviors of all the five types of penicillins at a boron-doped diamond electrode (BDDE), showing that all these drug

molecules can be oxidized at the high potential in the range from 1.4 to 1.8 V and that the BDDE could be applied for the electrochemical detection of those drugs in the real sample analysis. (Feier et al., 2017).

The modification of a GCE with graphene and poly(3,4-ethylenedioxythiophene (PEDOT) combined with AuNPs for the detection of penicillin exhibited high sensitivity with a detection limit of 57 ng L^{-1} (Zhao et al., 2016). Another electrochemical sensor based on the integration of Printex 6L Carbon (P6LC) and CdTe quantum dots (QDs) within a PEDOT:PSS (poly(3,4-ethylenedioxythiophene)-poly(styrene sulfonate)) film was prepared for the determination of amoxicillin (AMX) as illustrated in Fig. 6A (Wong et al., 2020). Fig. 6B presents the effect of pH on the electrochemical oxidation of AMX at the prepared sensor; the maximum peak current was achieved at pH 6.0. The interference study (Fig. 6C) demonstrated that the developed the QDs-P6LC-PEDOT:PSS/GCE sensor exhibited high selectivity and sensitivity for the detection of AMX. The electrochemical detection of penicillin G in milk via pulsed amperometric detection followed by HPLC, demonstrated a detection limit of 2 μM using a gold signal transducer (Kirchmann et al., 1994). This work improved the detection of penicillin G in the presence of other penicillin varieties and antibiotics by approximately a factor of 10. Li et al. fabricated a gold-based immunosensors with anti-penicillin G and a bilayer lipid membrane for the detection of traces of lower penicillin G at the value established by European Union (4 μg L^{-1}) (Li et al., 2015) Further, the designed sensor could be used as a sensing platform for the rapid screening of penicillin G. When compared with conventional HPLC, this sensor proved to be convenient and timesaving.

4.3.2 Tetracycline: Tetracycline (TET) has a wide range of anti-bacterial activities against gram-positive and gram-negative bacteria and is commonly employed in the agricultural sector as a food additive. Tang et al. designed a sensor for the detection of TET by combining particular DNA

aptamers and AuNPs with a molybdenum sulfite (MoS_2) and titanium dioxide (TiO_2) electrode. MoS_2 and TiO_2 was used as the binder between GCE and AuNPs; their spherical structure also provided a high surface area for the attachment of AuNPs (Tang et al., 2018). The proposed sensor served as an indirect electrochemical detection method for TET with a dynamic range from 10 nM to 50 μM and a LOD of 5 nM for a milk sample. In another work, Fe_3O_4/AuNPs with chitosan were fabricated stepwise and tested for the detection of TET using CV and EIS. It was applied for food analysis, showing a recovery of 95.9 % and a standard deviation of 1.86 %. The specificity and stability of the sensors were investigated using interference antibiotics such as penicillin, chloramphenicol, erythromycin, and gentamycin at various concentrations (Liu et al., 2016). Likewise, MWCNTs/AuNPs were used within a MIP to develop a TET sensor. Consequently, the electrode was designed to have a maximum number of imprinted sites with an increased electron transfer rate. Using CV, the electrode revealed a low LOD of 90 nM for TET with the enhanced electrocatalytic activity of the AuNPs. The selectivity of the sensor was analyzed in the presence of common interferents (e.g., nafcillin, oxytetracycline, and chloramphenicol), and it was found that the interference by oxytetracycline was higher in contrast to the other two molecules (Wang et al., 2011).

4.3.3 Kanamycin: Qin et al. amended a hierarchical nanoporous (HNP) Pt–Cu alloy and thionine functionalized graphene (GR-TH) as biosensing substrates. The aptamer specific to kanamycin was arranged on an HNP–PtCu/GR-TH/GCE using high-affinity interactions by the amine group of the aptamer and PtNPs. The sensor presented a complete linear range response within the concentration range from 0.001 to 100 nM and a low LOD of 0.86 pM for kanamycin (Qin et al., 2016). Furthermore, the sensor exhibited high selectivity toward kanamycin in the presence of interfering species (e.g., human chorionic gonadotropin, dopamine, and tyrosine) demonstrating its practical

applicability for the analysis of animal-derived food. The feasibility of a flexible graphene-based potentiometric sensor has garnered tremendous attraction for portable/wearable electronics applications (Yao et al., 2019). These authors utilized a kanamycin aptamer with the sequence 5′-AGATGGGGGTTGAGGCTAAGCCGA-3′ integrated within graphene paper for the selective detection of kanamycin. Upon optimization, the aptasensor gave an ultralow detection limit of 30.0 pg L^{-1} via the common reversible catalytic reaction of the analyte (kanamycin) induced by the DNase I. Moreover, the sensor also demonstrated good practical use and excellent stability in milk samples.

4.3.4 Chloramphenicol: Chloramphenicol (CAP) is a potential therapeutic agent against both gram-positive and gram-negative bacteria. Based on properties of rGO and palladium nanoparticles, an electrochemical sensor was developed for the analysis of CAP (Yi et al., 2019). This nanocomposite was characterized using a transmission electron microscope for its structure. Electrochemical characterization was accomplished using CV, and DPV verified this sensor to be a straightforward technique for the detection of real-world samples such us honey and tap water. The authors examined the effects of multiple parameters (e.g., modifier amount, accumulation time, scan rate, and electrolyte pH) and demonstrated enhanced stability, selectivity and a wide linear range for the detection of CAP using the developed electrochemical sensor. The reaction mechanism was proposed to be a two-electron and two-proton transfer process with the product being the nitroso derivatives of CAP. Chen et al. had fabricated an electrochemical sensor that involved a mixture of molybdenum sulfide/polyaniline nanocomposite (MoS_2/PANI), which exhibited a linear range across three orders of magnitude in addition to other remarkable electrochemical advantages (e.g., reproducibility, repeatability, and anti-fouling behavior). As such, its potential was confirmed for CAP detection under neutral pH (Chen et al., 2016). Recently, europium oxide (Eu_2O_3) has emerged

as a promising electrocatalyst for the detection of CAP. Rajaji et al. demonstrated that the Eu_2O_3/rGO nanocomposite possessed good electric conductivity, thermal stability, flexibility, and large electrochemically available surface area and enhanced the reproducibility and sensitivity for the detection of CAP in honey and fresh milk samples (Rajaji et al., 2019).

4.4 Anti-fungal drugs

Anti-fungal drugs (antimycotics) are employed to treat fungal infections by killing or controlling the growth of fungi in the host with low toxicity. The introduction of anti-fungal drugs can be internal or external, where the seriousness of fungal infections is based on their interactions with the hosts immune systems. For example, foot fungus is odourful but not harmful; however, fungal infections of the blood and in tissues can be fatal. This section discusses and elaborates on polyene, azole, and allylamine fungicides in various electrochemical sensing and biosensing applications for real-time analysis.

4.4.1 Natamycin: Natamycin is the only polyene type of drug approved for the treatment of fungal keratitis. Aki et al. investigated the electrochemical behavior of natamycin and reported a DPV detection of natamycin in commercially available capsules using a CPE (Aki et al., 2005). The proposed sensor exhibited a low LOD of 5.0 μM; and the analytical results were further validated by UV-Vis spectroscopy. Another approach for the detection of natamycin was developed by immobilizing SWCNTs on the poly(L-serine)/GCE surface. The electrochemical oxidation of natamycin at the prepared electrode was elucidated using CV at various scan rates and chronocoulometry, revealing that the oxidation process was adsorption-controlled. Accumulation at the open circuit potential for 180 s greatly increased the peak current and further lowered the detection limit (Ye et al., 2015). Fig. 7 shows the integrated graphene oxide/MWCNT sensor for the detection of natamycin, demonstrating strong linear sweep adsorptive stripping voltammetric

response (A & B), high stability (C) and high selectivity (D) (Yang et al., 2018). The modification of the SPCE with the MWCNT/platinum-doped cadmium sulfide nanocomposites was also designed to investigate the electrochemical detection of natamycin (Yousefi et al., 2018). The sensor showed a linear relationship between the natamycin concentration and anodic peak current in the concentration range from 0.2 to 70.0 μM with a LOD of 0.12 μM. The proposed Pt-CdS/MWCNT/SPCE sensor was further tested with a homogenized yogurt drink with the spiking of known concentration of natamycin, confirming that this method was reliable for the quantitative analysis of natamycin in the dairy industry.

4.4.2 Fluconazole: Fluconazole (FLU) is a fluorine attached bis-triazole, which is used as an anti-fungal agent for vaginal yeast infections by *Candida* and recurring *Candida* infections. It is also used as a prophylactic therapeutic drug for patients who have undergone bone marrow transplants. Gil et al. studied the redox behavior of FLU at the Pt electrode and the GCE surface, revealing a pH-dependent oxidation process, with a peak current increase at pH 8 at the anodic peak potential of ~0.85 V, which involved the loss of a triazolic ring electron, creating a radical-cation and a further dimerization step to generate a bis-compound product. The capacity of FLU to strongly adsorb to the electrode surface might compromise some analytical parameters such as sensitivity, linearity, and reproducibility using the electrochemical technique (Gil et al., 2011). To overcome this issue, a novel Fe_3O_4@PA-Ni@Pd/Chitosan nanocomposite modified carbon ionic liquid electrode was prepared for the sensitive detection of FLU as shown in Fig. 8 (Zad et al., 2018). Fig. 8A and B show the morphology, structure, and composition of the prepared nanocomposite. The multiple regression analysis was employed to optimize the experimental condition as illustrated in Fig. 8C, showing the dependence of the 3D response surface of the measured electrochemical current of FLU on the accumulation time and the nanoparticle concentration. Figure 8D displays the

CV responses of the fabricated sensor to FLU at different scan rates varied from 10 to 500 mV s^{-1}. The developed sensor exhibited a wide linear range from 0.01 to 400 μM with a LOD of 3.5 nM; it was also validated by measuring FLU in serum and urine samples, showing high selectivity (Zad et al., 2018).

4.4.3 Ketoconazole: This anti-fungal agent is used as an oral drug due to its low toxicity and versatile distribution throughout the bloodstream, urine, saliva, and joint fluids. Peng and co-workers investigated the electrochemical and adsorptive properties of ketoconazole at a GCE using CV, whereas DPV was employed for the electrochemical detection in the presence of possible interferent molecules, showing high sensitivity and selectivity (Peng et al., 2001). In another study, the electrochemical analysis of ketoconazole was conducted with the simultaneous detection of ciclopirox olamine (a pyridine anti-fungal agent which is used in cosmetics) using a BDDE. The optimal electrochemical oxidation of both drugs was studied using SWV, showing a linear dependence of 0.29 to 3.13 μM for ketoconazole, and from 25.3 to 419 μM for ciclopirox olamine. The pH studies revealed that an alkaline solution was favorable for the electrochemical qualitative and quantitative analyses of ketoconazole, while a neutral pH was better for the analysis of ciclopirox olamine (Mielech-ŁUkasiewicz and Rogińska, 2014).

4.4.4 Tolnaftate: Tolnaftate (TNF) is an anti-fungal agent that has been used over many decades for the treatment of different dermatophytes and multiple forms of microsporons, which primarily instigate several infectious tinea conditions (cruris, pedis, and capitis). Disposable SPEs were employed for the electroanalysis of TNF, offering a sensitive and reproducible electrochemical platform for the detection of TNF and its active hydrolysis products. A well explainable irreversible oxidation was observed at 1.20 V with a linear range from 0.24 to 3.76 μM under different pH

ranging from 2 to 10. The electrooxidation involved a single electron transfer with the release of a water molecule and was proven to be a diffusion-controlled process (Khairy and Khorshed, 2020).

4.4.5 Clioquinol: Clioquinol (CQL) is a topical drug used to address intestinal fungal infections and subacute myeloid-optic neuropathies. The application of tin molybdate $(SnMoO_4)_2$ nanoplates for the electrochemical detection of CQL exhibited improved sensitivity, good stability and high selectivity (Raj Karthik et al., 2017). This sensor showed a LOD of 14 nM in the presence of a number of common metal ions, such as 50-fold concentration of Cu^{2+}, Fe^{2+}, K^+, Ca^{2+}, Na^+, Cl^-, Br^-, and I^-; 20-fold concentration of biologically interfering substances such as dopamine, uric acid, ascorbic acid , and glucose; and 20-fold excess concentration of some commonly used drugs in a mixture, including CAP, acetaminophen, amoxicillin, and metronidazole. Likewise, three-dimensional flower-like cerium vanadate ($CeVO_4$) was employed for the real-time monitoring of CQL in biological samples. The electrocatalytic activity of the $CeVO_4$ modified SPCE for the electrochemical detection of CQL was evaluated by CV and DPV. This approach also showed a low oxidation peak potential (+0.47 V) together with a wide linear range 0.02 to 2.15 mM and a low detection limit of 0.004 μM in the presence of the interferent molecules 4-nitroaniline, 4-nitrobenzene, nitromethane, methyl parathion, CAP and imipramine (Kokulnathan et al., 2019b). They also proposed another carbon-metal based (EuV/GO) electrochemical sensor for the detection of CQL with the linear range from 0.005 to 331 μM and a LOD of 1.0 nM. The successive utilization of the fabricated electrode for the analysis of the spiked CQL (known concentration) in human urine samples revealed a recovery range of 97.5 to 105 % for different concentration, showing that the developed sensor could be used in various electrochemical sensing application (Kokulnathan and Chen, 2019).

4.5 Anti-viral drugs

Anti-viral drugs comprise a group of medications that are used to treat all types of viral-based infections ranging from flu viruses to human immunodeficiency viruses. Most viral drugs are administered intravenously rather than orally. The overdosing of anti-viral drugs may make the body resistant to the treatment of other viral infections; thus, quantitative and qualitative analysis is critical. In this section, the electrochemical sensing of several commonly used anti-viral drugs such as acyclovir (ACV), ganciclovir (GCV), zanamivir (ZAV), valacyclovir (VCV), oseltamivir, and abacavir is highlighted.

4.5.1 Acyclovir: ACV is an intravenous and oral drug for the treatment of many viral infections such as herpes simplex, hepatitis B virus, and varicella zoster virus. The synergy between MWCNT-dihexadecyl hydrogen phosphate (DHP) enabled the enhanced direct electrochemical detection of ACV in a wide linear range from 0.08 to 10.0 μM, and a detection limit of 0.03 μM. The hollow nanostructured film electrode showed enhancement in the electrochemical detection of ACV by its high electrochemical active surface area. The proposed sensing platform was applied for the analysis of a commercially available ACV tablet, showing promising practical application. The voltammetric detection of ACV at a fullerene-C_{60}-modified GCE delivered remarkable electrocatalytic activity with an increase of the peak current and a decrease of the peak potential for both pharmaceutical and biological samples. The LOD and limit of quantitation (LOQ) were found to be 0.015 and 0.049 μM, respectively (Wang et al., 2006). Wang et al. modified a CPE with polyvinylpyrrolidone (PVP) and a macromolecule surfactant (Wang et al., 2013). The PVP-modified CPE electrode notably increased the oxidation signal, compared to an unmodified CPE. The electrochemical oxidation involved a two-electron and two-proton process with a LOD of 2.5 nM. Several parameters such as pH, accumulation time, accumulation potential, and the PVP concentration were optimized for the electrochemical detection of ACV. To verify accuracy, the

concentration of ACV used for electrochemical analysis was compared with the HPLC analysis, showing a good agreement. Recently, a facile electrochemical method was proposed for the detection of ACV using PGEs with a low LOD of 0.3 μM. The electrochemical oxidation of ACV on the PGE had a multistep irreversible oxidation process and the final products were radicalic hydroxy-guanine and oxo-guanine (Dilgin and Karakaya, 2016).

4.5.2 Ganciclovir: GCV is a clinically approved drug for the treatment against cytomegalovirus, herpes virus and Epstein-Barr virus. Electrochemical oxidation at a GCE was confirmed to be a simple, rapid, and sensitive approach for the detection of GCV in serum and pharmaceutical samples (Uslu et al., 2005). Quantitative evaluation was accomplished through DPV and SWV at pH 2.0 in the concentration range between 1.0 and 100.0 μM. The electrochemical oxidation of guanine moiety was the key step which led to the increase in the peak current, while the interference molecules could not be oxidized at the potential of GCV oxidation. In another work, a boron-doped nanocrystal diamond (BDND) electrode showed excellent performance for the detection of GCV at pH 2.5; the peak current at 1.2 V increased linearly with the increase of the concentration using DPV. In addition, the BDND sensor exhibited much higher stability over GCE, due to fewer oxygen groups generated during the electrochemical oxidation, which mitigated fouling (Zhou et al., 2011). The electrochemical oxidation of GCV is irreversible along with a two-electron and two-proton transfer using Au nanoparticles and MWCNT composites. Fig. 9A illustrates the procedure for the preparation of the sensor and the structure of the MIP. Fig. 9B displays the bar graph of interference analysis of target molecule with the other molecules present in real samples. Fig. 9B displays the CVs of 100 μM GCV at different electrodes, revealing that the AuNPs/MIP/MWCNT/GCE had higher activity for the electrochemical oxidation of GCV. As seen in Fig. 9C, the imprinted AuNPs/MIP/MWCNT/GCE sensor exhibited special recognition to GCV and high selectivity. The

LOD and LOQ were found to be 0.0015 and 0.005 μM, respectively, demonstrating high sensitivity (Gholivand and Karimian, 2015).

4.5.3 Zanamivir: ZAV is a new drug that is used against influenza A H5N1 and H1N1 viruses. Although ZAV is a biologically interesting compound, its electrochemical analysis has not been explored mush as yet due to its being the latest addition to the anti-viral drug family. Skrzypek investigated the electrochemical oxidation of ZAV at a mercury dropped electrode using square wave adsorptive stripping voltammetry, revealing that the electrochemical oxidation process was pH sensitive and that the maximum peak current was obtained at a pH of 2.2 (Skrzypek, 2010). Wahyuni et al. proposed an Au-based sensor for the detection of neuraminidase (NA), which is an exosialidase enzyme present in some viruses, based on the electrochemical oxidation of ZAV. The reason for this is that although NA is not directly oxidized electrochemically, its attachment to ZAV shifts the peak potential for the ZAV oxidation allowing for the indirect detection of NA (Wahyuni et al., 2015).

4.5.4 Valacyclovir and acetaminophen*:* The use of multiple drugs is a common clinical practice to overcome infections and various side effects. In the case of viral invasion, the application of both anti-viral and antipyretic drugs can serve as assets in the fight against infections. However, for this scenario the regular monitoring of both drugs is required. Therefore, the simultaneous and sensitive detection of VCV and acetaminophen was proposed based on rGO. Figure 10A and B display the SEM image of the rGO formed on a GCE and the EDX spectra of GO and rGO. Figure 10C compares the CVs of VCV and acetaminophen recorded at the GCE and rGO/GCE, revealing the possibility for the simultaneous detection of VCV and acetaminophen using the rGO/GCE. Figure 10D shows the strong DPV responses of the rGO/GCE to the successive addition of both acetaminophen and VCV with the LOD of 4.65 nM and 3.1 nM, respectively (Adhikari et al.,

2016). The electrochemical oxidation involves a two-electron and two-proton process to form 8-oxovalacyclovir as the final product. The reaction was determined to be irreversible and diffusion-controlled.

4.6 Anti-cancer drugs

Anti-cancer drugs have their functionality in terms of eliminating cancer cells, shrinking tumours, preventing cancer from metastasizing and spreading, and relieving various cancer symptoms. Based on the aforementioned criteria, various anti-cancer drugs have been developed. The continuous production and regular clinical application of these drugs require ready-to-use qualitative and quantitative analysis platforms. This section highlights some recent advances in the electrochemical sensing of anti-cancer drugs.

4.6.1 Taxol: Taxol is derived from the natural compounds present in the stem bark of the Pacific yew tree, which is known to be an effective drug against ovarian cancer, breast cancer, and non-small-cell lung cancer. An analytical method was designed for the determination of Taxol via cathodic stripping SWV. The detection of Taxol was achieved under alkali conditions using a mercury drop electrode with a 0.0278 cm^{-2} electroactive surface area (Holgado et al., 2003). Efforts to develop and improve Taxol sensors have been primarily based on DPV using PGEs, where Taxol was determined through its interaction with salmon-sperm double stranded DNA (ds-DNA). In the applied potential range from 0.5 to 1.3 V, the interaction reduced the intensity of the guanine and adenine oxidation signals through which the Taxol electroanalysis was achieved with a linear range from 0.2 to 10.0 μM (Taei et al., 2015). Another study by Tajik et al. modified the PGE surface with a carbon/metal-oxide/polymer (ds-DNA-MWCNT-TiO_2/ZrO_2–CHITOSAN) nanocomposite. The voltammetric oxidation of Taxol was increased by the favorable electron transfer properties and high active sites. This synthesized nanocomposite electrode served as a sensitive, stable, and selective sensing platform for the detection

of Taxol with a linear range from 0.7 nM to 1.87 μM and a low detection limit of 0.01 nM (Tajik et al., 2015).

***4.6.2 Doxorubicin*:** Doxorubicin is an anthracycline drug extracted from *Streptomyces peucetius var. caesius*, which is used in the treatment of various types of leukemia, as well as lung and breast cancers. The rapid and sensitive analysis of doxorubicin was explored using a carbon disk working electrode. The proposed mechanism behind the electrochemical catalysis was a pseudo-reversible reaction in an acetate buffer, which was confirmed by a well-defined single peak that shifted toward negative potentials as the pH values were increased (Hahn and Lee, 2004). Clinical and environmental applications were the final aims in the design of these sensors. For this purpose, Nicole and coworkers developed a detection technique for doxorubicin using artificial single-stranded nucleic acids with the capacity to bind with target molecules (aptasensor). The analysis proceeded under a wide concentration range from 4 to 1000 nM, where the saturation of the aptamer adhered gold electrode occurred at 125 nM (Bahner et al., 2018). The simultaneous detection of two different drugs contributes to the cost effectiveness and time saving aspects of a given sensing platform. For example, the simultaneous detection of doxorubicin and another anti-cancer drug (methotrexate) was attempted to be developed for drug analysis with application in biological, clinical, and pharmaceutical domains. A cyclodextrin-graphene hybrid nanocomposite on a GCE (CD-GN/GCE) was synthesized for the simultaneous detection of doxorubicin and methotrexate. The peak currents of doxorubicin and methotrexate on the CD-GN/GCE increased by 26.5 and 23.7 fold, respectively, in comparison to the results obtained on a bare GCE (Guo et al., 2011). Another DNA/noble metal (DNA/silver) based sensor, fabricated for the detection of doxorubicin using solid state voltammetry as depicted in Fig. 11A. The TEM images of the silver NPs before and after the conjugation with doxorubicin are presented in Figure 11B, confirming that the dimension of the Ag NPs remained the same after conjugation.

The comparison of voltammetric results measured in 0.3 M of KCl when a doxorubicin loading per AgNP of (red line) ~17 and (black line) ~1 was used in the labeling process, showing that the sensitivity decreased with the increase of doxorubicin loading because of its unfavourable intercalation (Ting et al., 2009).

***4.6.3 Imatinib and flutamide*:** Imatinib (IMA) is an anti-cancer drug for chronic myeloid leukemia (CML) and gastrointestinal stromal tumors (GISTs). The monitoring of this drug is required in biological fluids such as blood, cerebrospinal fluid, plasma, and urine. On the basis of the above-mentioned requirements, a dendrimer layered hollow fibre graphene oxide sensor was developed for the simultaneous microextraction and electrochemical detection of IMA in biological samples (Hatamluyi and Es'haghi, 2017). An interference study was conducted using three anti-cancer drugs (Nilotinib, Ponatinib, and Dasatinib), which exhibited high selectivity toward the IMA, with a detection limit of 7.39 nM. SPCEs were used in making the sensor as they are known to enable easy, fast activating, and low-cost sensors for the quantitative detection of many drugs (Rodríguez et al., 2018). For example, the voltammetric detection of IMA was achieved using SPCEs (CNT) and showed the oxidation behaviour of IMA at a piperazine ring at a peak potential of 0.75 V. This electrode mechanism indicated that the catalytic process was irreversible without further reduction visualised from the significant increase of current from 0.71 V and followed a typical adsorption-controlled process. Further, this designed electrode was compared to platinum and gold working electrodes, where both electrodes failed to reach the efficacy of the SPCEs for the detection of IMA. When immunocompromised patients are treated, various drugs are administered either orally, muscularly, or intravenously. In this scenario one drug may supress the activity of another drug, which might result in serious side effects or alterations to dosage may be required. To avoid these complications, simultaneous drug detection is desirable. The simultaneous detection of an anti-cancer (IMA) and an

anti-fungal agent (Itraconazole) was facilitated using a metal-oxide/carbon-based electrode (NiO-ZnO/MWCNT-COOH/GCE). DPV showed that an increase in the oxidation peak current for itraconazole with a LOD of 4.1 nM and good sensitivity of 2.64 μA μM^{-1} cm^{-2}. The linearity range of IMA was 0.015 – 2.0 μM with a LOD of 2.4 nM and a sensitivity of 9.64 μA μM^{-1} cm^{-2} (Chen et al., 2019). Most recently, Tseng et al. proposed a graphene oxide sheet calcium titanium oxide (GOS/$CaTiO_3$) based nanocatalyst for the electrochemical detection of flutamide, the non-steroidal antiandrogen used for the treatment of prostate cancer and leukemia. Fig. 12A, B and C present the morphology, structure and composition of the formed nanocatalyst based on the XRD, TEM and EDX surface characterization. Fig. 12D and E display the i-t response to flutamide and the associated calibration plot, showing a wide linear range (0.015 to 1184 μM), a low LOD (5.7 nM) and high sensitivity (1.073 μA μM^{-1} cm^{-2}). The sensor was further tested with human blood and urine samples, confirming the promising application for the anti-cancer drug detection (Tseng et al., 2020).

5. Conclusion and Outlook

Given the increased demand for rapid, accurate, and cost-effective techniques for the detection and quality control of pharmaceutical compounds over the last decade, considerable interest and significant progress have been made toward the development of dedicated nanomaterial-based electrochemical sensors and biosensors. A thorough elucidation of the physicochemical and electronic interactions that occur at the interfaces between nanomaterials and analytes of interest is necessary for exploiting the full potential of developed electrochemical sensors. This comprehensive review covers the latest advances in the development of nanomaterial-based electrochemical sensors for the detection of six classes of significant pharmaceutical drugs as summarized in Table 1. The molecular structures of

these pharmaceutical compounds, as well as the nanomaterials, electrochemical methods employed, and the associated linear ranges and LOD of recently developed sensors and biosensors are compared in the table. Notably, significant progress has been made towards the integration of carbon-based nanomaterials with metal nanoparticles, quantum dots, organic functional groups, and conductive polymers with the aim of creating robust synergetic effects to facilitate catalytic reactions with target analytes. While this approach appears to be promising (sensitivity and LOD were improved in many cases), it leads to other issues such as fouling and the non-specific adsorption of other species, which make the proposed electrochemical sensors more difficult to apply commercially. Indeed, some researchers have questioned whether the incorporation of carbon-based nanomaterials such as graphene, GO, and CNTs generated synergetic effects for the electrochemical detection of analytes. For instance, in some cases, although a sensor that incorporated carbon nanomaterials with metal nanoparticles, organic functional groups, conductive polymers, or other modifications exhibited good performance, it was not conclusively verified whether the carbon nanomaterials or the modified materials themselves, might produce a comparable signal. Furthermore, the enhanced performance observed upon modification with carbon nanomaterials might simply be due to an increase of the electrochemically active surface area. Moreover, an intrinsic lack of understanding regarding GO-based nanomaterials might cause inaccurate attributions of the sensor's performance. For example, it was revealed that the oxygen content (e.g., epoxy, hydroxyl, carboxylic functional groups) was a critical factor that affected the catalysis of organic molecules. A higher oxygen content may increase or decrease the performance of electrochemical sensors depending on the analyte. This should be taken account when developing GO/rGO based nanomaterials, as the incorporation of other modified materials may be of secondary importance. Notably, while there are various promising electrochemical sensors proposed for each class of pharmaceutical compounds, there are some trends as to which kind of nanomaterials may be

more effective. For small molecular pharmaceuticals such as aspirin, ibuprofen and sertraline, nanoparticle or organic molecule functionalized electrodes exhibited a low LOD and high-performance. On the other hand, for large molecular drugs such as naproxen, diclofenac, paroxetine, fluoxetine and venlafaxine, carbon nanomaterials or carbon-based nanocomposites seem to be more effective. The large molecules usually have multiple aromatic rings, which make the reaction sites of the analyte less accessible for specific interactions with the sensor interfaces. A thorough understanding of the electrochemical reactions at electrode/electrolyte interfaces remains a major challenge for tailoring the design of sensing platforms. Although most proposed electrochemical sensors were tested with real samples such as urine, blood and other biological fluids, there is a considerable gap between the lab tests and the fabrication of sensing devices for practical and commercial applications. Specialized electrochemistry researchers may not possess the necessary expertise to develop fully functional sensors that integrate sensing elements, transducers, programming, the building of electronic components, and so on. Therefore, joint efforts from industry and multidisciplinary research groups are of crucial importance for the development and commercialization of electrochemical sensors and biosensors for the effective detection of pharmaceutical compounds. aside from the sensitivity and selectivity, the costs and stability of electrochemical sensors/biosensors must be carefully evaluated.

Currently, chromatographic techniques (e.g., HPLC, UPLC, GC-MS and LC-MS/MS) and colorimetric methods have been commonly used in hospitals and labs for the analysis of pharmaceuticals. Although satisfactory results can be obtained, expensive instruments and well-trained personnel are required. In addition, those techniques are often limited by their portability. In contrast, electrochemical sensors have the advantages to overcome the drawbacks of those conventional techniques. One of the emerging trends is to integrate the electrochemical sensing with liquid chromatography or mass spectrometry for the efficient detection of pharmaceuticals. The

intermediates and products generated from electrochemical oxidation/reduction of the analyte may be further quantified by liquid chromatography or mass spectrometry. In summary, significant progress has been made towards the development of advanced electrochemical sensors/biosensors for the detection of pharmaceutical compounds over the last decades. Nanocomposites comprised of carbon and other nanomaterials such as metal nanoparticles, polymers, and functionalized nanostructures are a promising trend to further enhance the sensitivity and lower the limits of detection for target analytes through synergistic effects. MIP has become increasingly popular in recent years, which may be attributed to more complete understanding of analytes and the nanomaterials employed, through various experimental data and theoretical computations. Descriptions of strategies for the development of these electrochemical sensors, which are tuned for specific analytes, aim to provide readers and scientists with an extensive toolbox for the detection of a wide array of pharmaceuticals. We hope to inspire and motivate readers by contributing to the establishment of a solid understanding of existing nanomaterials for the sensing of pharmaceuticals, as well as to provide examples of the opportunities and applications that these devices can create for the advanced sensing of pharmaceutical compounds, to protect human health and ensure environmental safety.

Credit authorship contribution statement

Lanting Qian: Methodology, Data curation, Formal analysis, Writing - original draft. **Sharmila Durairaj**: Methodology, Formal analysis, Writing - original draft; **Scott Prins**: Visualization, Writing - review & editing. **Aicheng Chen**: Conceptualization, Supervision, Funding acquisition, Writing - review & editing.

Declaration of competing interest

No conflict of interest for this work.

Acknowledgement

This work was supported by a Discovery grant from the Natural Sciences and Engineering Research Council of Canada (NSERC RGPIN-06248). A.C. acknowledges NSERC and the Canada Foundation for Innovation (CFI) for the Canada Research Chair Award in Electrochemistry and Nanoscience.

References

Abdel-aal, F.A.M., Rageh, A.H., Said, M.I., Saleh, G.A.,. Anal. Chim. Acta 1038 (**2018**) 29–40.

Adhikari, B.R., Govindhan, M., Chen, A., Sensors 15 (**2015**) 22490-22508.

Adhikari, B.R., Govindhan, M., Schraft, H., Chen, A., 2016. J. Electroanal. Chem. 780 (**2016**) 241–248.

Ahmadi, F., Raoof, J.B., Ojani, R., Baghayeri, M., Lakouraj, M.M., Tashakkorian, H., Cuihua Xuebao/Chinese J. Catal. 36 (**2015**) 439–445.

Akhter, S., Basirun, W.J., Shalauddin, M., Johan, M.R., Bagheri, S., Akbarzadeh, O., Anuar, N.S., Mater. Chem. Phys. 253 (**2020**) 123393.

Aki, C., Yilmaz, S., Dilgin, Y., Yagmur, S., Suren, E., Pharmazie 60 (**2005**) 747–750.

Alizadeh, T., Azizi, S., Biosens. Bioelectron. 81 (**2016**) 198-206

Allahverdiyeva, S., Keskin, E., Pınar, P.T., Yunusoğlu, O., Yardım, Y., Şentürk, Z., Diam. Relat. Mater. 108 (**2020**) 107962.

Alqarni, S.A., Hussein, M.A., Ganash, A.A., Khan, A., Bionanoscience. 10 (**2020**) 351-364.

Amin, S., Soomro, M.T., Memon, N., Solangi, A.R., Sirajuddin, Qureshi, T., Behzad, A.R., 2014. Environ. Nanotechnology, Monit. Manag. 1 (**2014**) 8-13.

Ardelean, M., Pode, R., Schoonman, J., Pop, A., Manea, F. WIT Trans. Ecol. Environ. 216 (**2017**) 213-220.

Arkan, E., Karimi, Z., Shamsipur, M., Saber, R., 2013. Anal. Sci. 29 (**2013**) 855-60.

Atta, N.F., Galal, A., Ahmed, Y.M., J. Electroanal. Chem. 838 (**2019**) 107–118.

Azab, S.M., Fekry, A.M., New J. Chem. 41(**2017**) 11846–11852.

Bahner, N., Reich, P., Frense, D., Menger, M., Schieke, K., Beckmann, D., Anal. Bioanal. Chem.

410 (**2018**) 1453–1462.

Bai, J., Zhou, B., Chem. Rev. 114 (**2014**) 10131-10176.

Baj-Rossi, C., Rezzonico Jost, T., Cavallini, A., Grassi, F., De Micheli, G., Carrara, S., Biosens. Bioelectron. 53 (**2014**) 283-7.

Bakshi, S.R., Lahiri, D., Agarwal, A.Int. Mater. Rev. 55 (**2013**) 41-64.

Bandyopadhyay, A., Ghosh, D., Pati, S.K., Phys. Chem. Chem. Phys. 19 (**2017**) 24059-24066.

Baptista, F.R., Belhout, S.A., Giordani, S., Quinn, S.J., Chem. Soc. Rev. 44 (**2014**) 4433-4453.

Bard, A.J., Faulkner, L.R., 2001 2nd Ed. John Wiley&Sons, New Jersey, USA.

Basu, S., Bhattacharyya, P., Sensors Actuators B Chem. 173 (**2012**) 1-21.

Beitollahi, H., Yoonesfar, R.,Anal. Bioanal. Electrochem. 8 **(2016)** 29-37

Bell, A.T., Science 299 (**2003**) 1688-1691.

Bridle, H, 2000. 3nd Ed. Elsevier, Amsterdam, Netherlands.

Boles, M.A., Ling, D., Hyeon, T., Talapin, D. V., Nat. Mater. 15 (**2016**) 141-153.

Bracey, C., Ellis, P., Hutchings, G., Chem. Soc. Rev. 38 (**2009**) 2231-2243.

Brycht, M., Skrzypek, S., Karadas-Bakirhan, N., Smarzewska, S., Bozal-Palabiyik, B., Ozkan, S.A., Uslu, B., 2015. V Ionics, 21 (**2015**) 2345-2354.

Camilli, L., Passacantando, M., 2018. Chemosensors 6 (**2018**) 62

Chen, A., Chatterjee, S., Chem. Soc. Rev. 42 (**2013**) 5425.

Chen, A., Shah, B., 2013. Anal. Methods 5 (**2013**) 2158-2173.

Chen, H., Luo, K., Li, K., J. Electrochem. Soc. 166 (**2019**) B697–B707.

Chen, H.Y., Wang, J., Meng, L., Yang, T., Jiao, K., Chinese Chem. Lett. 27 (**2016**) 231–234.

Chen, X., Mao, S.S., Chem. Rev. 107 (**2007**) 2891-2959.

Chethana, B.K., Basavanna, S., Arthoba Naik, Y.,Ind. Eng. Chem. Res. 51 (**2012**) 31.

Cincotto, F.H., Golinelli, D.L.C., Machado, S.A.S., Moraes, F.C., Sensors Actuators B Chem. 239 **(2017**) 488-493.

Compton, R.G., Banks, C.E., 2007, World Scientifics, Singapore.

Dai, H., Xu, G., Gong, L., Yang, C., Lin, Y., Tong, Y., Chen, J., Chen, G., Electrochim. Acta 80 (**2012**) 362–367.

Danesh, N.M., Ramezani, M., Emrani, A.S., Abnous, K., Taghdisi, S.M., Biosens. Bioelectron. 75 (**2016**) 123–128.

De S. Gil, É., Cordeiro, D.D., Matias, A.E.B., Serrano, S.H.P., J. Braz. Chem. Soc. 22 (**2011**) 767–771.

Deiminiat, B., Razavipanah, I., Rounaghi, G.H., Arbab-Zavar, M.H., Sensors Actuators B Chem. 244 (**2017**) 785-795.

Deroco, P.B., Rocha-Filho, R.C., Fatibello-Filho, O., Talanta 179 (**2018**) 115–123.

Devarushi, U.S., Shetti, N.P., Bukkitgar, S.D., Tuwar, S.M., Russ. J. Electrochem. 54 (**2018**) 760–768.

Dilgin, D.G., Karakaya, S., Mater. Sci. Eng. C 63 (**2016**) 570–576.

Diouf, A., Moufid, M., Bouyahya, D., Österlund, L., El Bari, N., Bouchikhi, B., Mater. Sci. Eng. C.110 (**2020**) 110665.

Donarelli, M., Ottaviano, L., Sensors 18 (**2018**) 3638-3683.

Duan, H., Wang, D., Li, Y., Chem. Soc. Rev. 44 (**2015**) 5778-5792.

Duclaux, L., 2002. Carbon 40 (**2002**) 1751-1764.

Dumestre, F., Chaudret, B., Amiens, C., Renaud, P., Fejes, P., Science 303 (**2004**) 821-823

El-badawy, F.M., Mohamed, M.A., El-Desoky, H.S., Microchem. J. 157 (**2020**) 104914.

El-Wekil, M.M., Mahmoud, A.M., Alkahtani, S.A., Marzouk, A.A., Ali, R., Biosens. Bioelectron. 109 (**2018**) 164–170.

Elgrishi, N., Rountree, K.J., McCarthy, B.D., Rountree, E.S., Eisenhart, T.T., Dempsey, J.L., J. Chem. Educ. 95 (**2018**) 197-206.

Espinosa, E.H., Ionescu, R., Chambon, B., Bedis, G., Sotter, E., Bittencourt, C., Felten, A., Pireaux, J.J., Correig, X., Llobet, E., Sensors Actuators, B Chem. 127 (**2007**) 137-142.

Fasipe, O., 2018. Arch. Med. Heal. Sci. D 6 (**2018**) 81-94.

Feier, B., Ionel, I., Cristea, C., Săndulescu, R., New J. Chem. 41 (**2017)** 12947–12955.

Ferreira, L.M.C., Felix, F.S., Angnes, L., Electroanalysis 24 (**2012**) 961–966.

Fouladgar, M., Hadjmohammadi, M.R., Khalilzadeh, M.A., Biparva, P., Teymoori, N., Beitollah, H., Int. J. Electrochem. Sci. 6 (**2011**) 1355–1366.

Ghadimi, H., M.A.Tehrani, R., Basirun, W.J., Ab Aziz, N.J., Mohamed, N., Ab Ghani, S.,J. Taiwan Inst. Chem. Eng. 65 (**2016**) 101-109.

Gholivand, M.B., Karimian, N., Sensors Actuators B Chem. 215 (**2015**) 471–479.

Gowda, J.I., Nandibewoor, S.T., Electrochim. Acta 116 (**2014a**) 326–333.

Gowda, J.I., Nandibewoor, S.T., Asian J. Pharm. Sci. 9 (**2014b**) 42–49.

Guo, Y., Chen, Y., Zhao, Q., Shuang, S., Dong, C., Electroanalysis 23 (**2011**) 2400–2407.

Guo, Y., Shen, G., Sun, X., Wang, X., IEEE Sens. J. 15 (**2015**) 1951–1958.

Hahn, Y., Lee, H.Y., Arch. Pharm. Res. 27 (**2004**) 31–34.

Hall, A.J., Logan, J.E., Toblin, R.L., Kaplan, J.A., Kraner, J.C., Crosby, A.E., Pharmaceutical Overdose Fatalities. Jama. 300 (**2008**) 2613-20.

Hatamluyi, B., Es'haghi, Z., J. Electroanal. Chem. 801 (**2017**) 439–449.

He, Y., Wang, X., Huang, W., Chen, R., Zhang, W., Li, H., Lin, H., Chemosphere 193 (**2018**) 89-99.

Heiligtag, F.J., Niederberger, M., Mater. Today.16 (**2013**) 262-271.

Heli, H., Zarghan, M., Jabbari, A., Parsaei, A., Moosavi-Movahedi, A.A., J. Solid State Electrochem. 14 (**2010**) 787–795.

Holgado, T.M., Quintana, M.C., Pinilla, J.M., Microchem. J. 74 (**2003**) 99–104.

Ibrahim, H., Temerk, Y., Farhan, N., Talanta 179 (**2018**) 75–85.

Ivandini, T.A., Ariani, J., Jiwanti, P.K., Gunlazuardi, J., Saepudin, E., Einaga, Y., Makara J. Sci. 21 (**2017**) 34-42.

Ivandini, T.A., Sarada, B. V., Terashima, C., Rao, T.N., Tryk, D.A., Ishiguro, H., Kubota, Y., Fujishima, A., J. Electroanal. Chem. 512 (**2002**) 117-126.

Jankowska-Ꝉiwińska, J., Dawgul, M., Pijanowska, D.G., Procedia Engineering, 120 (**2015**) 574-577.

Jia, N., Cao, L., Wang, Z., Langmuir 24 (**2008**) 5932-5936.

Joghani, R.A., Rafati, A.A., Ghodsi, J., Assari, P., Feizollahi, A., J. Appl. Electrochem. 50 (**2020**) 1199-1208.

Joseph, R., Kumar, K.G., Anal. Sci. 27 (**2011**) 67–72.

Jung, D., Kim, J., Lee, G.S., 2015. Sensors Actuators A Phys. 223 (**2015**) 11-17.

Karthik, R., Govindasamy, M., Chen, S.M., Chen, T.W., Vinoth Kumar, J., Elangovan, A.,

Muthuraj, V., Yu, M.C., RSC Adv. 7 (**2017a**) 25702–25709.

Karthik, R., Sasikumar, R., Chen, S.M., Vinoth Kumar, J., Elangovan, A., Muthuraj, V., Muthukrishnan, P., Al-Hemaid, F.M.A., Ajmal Ali, M., Elshikh, M.S., J. Colloid Interface Sci. 487 (**2017b**) 289–296.

Karthik, Raj, Vinoth Kumar, J., Chen, S.M., Seerangan, K., Karuppiah, C., Chen, T.W., Muthuraj, V., ACS Appl. Mater. Interfaces 9 (**2017**) 26582–26592.

Kerr, G.W., McGuffie, A.C., Wilkie, S., Emerg. Med. J. 18 (**2001**) 236-241.

Kesavan, G., Chen, S.M., Diam. Relat. Mater. 108 (**2020**) 107975.

Khairy, M., Khorshed, A.A., J. Electroanal. Chem. 871 (**2020**) 114274.

Khalilzadeh, M.A., Tajik, S., Beitollahi, H., Venditti, R.A., Ind. Eng. Chem. Res. 59 (**2020**) 4219-4228.

Khosrokhavar, R., Motaharian, A., Milani Hosseini, M.R., Mohammadsadegh, S., Microchem. J. 159 (**2020**) 105348.

Kirchmann, E., Earley, R.L., Welch, L.E., J. Liq. Chromatogr. 17 (**1994**) 1755–1772.

Knihnicki, P., Wieczorek, M., Moos, A., Kościelniak, P., Wietecha-Posłuszny, R., Woźniakiewicz, M., Sensors Actuators B Chem. 189 (**2013**) 37-42.

Knoth, H., Scriba, G.K.E., Buettner, B., Pharmazie 70 (**2015**) 374–378.

Kokulnathan, T., Chen, S.M., ACS Sustain. Chem. Eng. 7 (**2019**) 4136–4146.

Kokulnathan, T., Karthik, R., Chen, S.M., Kumar, J.V., Sakthinathan, S., Microchim. Acta 186 (**2019a**.) 579.

Kokulnathan, T., Sakthi Priya, T., Wang, T.J., ACS Sustain. Chem. Eng. 7(**2019b**) 16121–16130.

Kong, X.K., Chen, C. Le, Chen, Q.W., Chem. Soc. Rev. 43 (**2014**) 2841-2857.

Kruanetr, S., Pollard, P., Fernandez, C., Prabhu, R., Int. J. Electrochem. Sci. 9 (**2014**) 5699-5711.

Lahav, M., Sehayek, T., Vaskevich, A., Rubinstein, I., Angew. Chemie - Int. Ed. 42 **(2003**) 5576-5579.

Lapworth, D.J., Baran, N., Stuart, M.E., Ward, R.S., Environ. Pollut. 163 (**2012**) 163-287.

Latif, I.A., Merza, S.H., Nanosci. Nanotechnol. 6 (**2016**) 24–33.

Leech, D., Wang, J., Smyth, M.R., 1990. Analyst 115 **(1990**) 1447–1450.

Li, H., Wei, Q., He, J., Li, T., Zhao, Y., Cai, Y., Du, B., Qian, Z., Yang, M., Biosens. Bioelectron.

26 (**2011**) 3590-5.

Li, H., Xu, B., Wang, D., Zhou, Y., Zhang, H., Xia, W., Xu, S., Li, Y., J. Biotechnol. 203 (**2015**) 97–103.

Li, Y., Zhao, X., Li, P., Huang, Y., Wang, J., Zhang, J.,. Anal. Chim. Acta. 884 (**2015**) 106-13.

Li, Z., Liu, C., Sarpong, V., Gu, Z., Biosens. Bioelectron. 126 (**2019**) 632–639.

Lima, A.B., Faria, E.O., Montes, R.H.O., Cunha, R.R., Richter, E.M., Munoz, R.A.A., dos Santos, W.T.P., Electroanalysis 25 **(2013**) 1585-1588.

Liu, B., Tang, D., Zhang, B., Que, X., Yang, H., Chen, G., Biosens. Bioelectron. 41(**2013**) 551–556.

Liu, B., Zhang, B., Cui, Y., Chen, H., Gao, Z., Tang, D., ACS Appl. Mater. Interfaces 3(**2011**) 4668–4676.

Liu, X., Hu, M., Wang, M., Song, Y., Zhou, N., He, L., Zhang, Z.,. Biosens. Bioelectron. 123 (**2019**) 59–68.

Liu, X., Zheng, S., Hu, Y., Li, Z., Luo, F., He, Z., Food Anal. Methods 9 (**2016**) 2972–2978.

Liu, Z., Forsyth, H., Khaper, N., Chen, A., Analyst 141 (**2016**) 4074-4083.

Long, F., Zhang, Z., Wang, J., Yan, L., Zhou, B., Electrochim. Acta 168 (**2015**) 337-345

Lu, C., Huang, P.J.J., Liu, B., Ying, Y., Liu, J., Langmuir 32 (**2016**) 10776–10783.

Maduraiveeran, G., Sasidharan, M., Ganesan, V., Biosens. Bioelectron. 103 (**2018**) 113–129.

Mailu, S.N., Waryo, T.T., Ndangili, P.M., Ngece, F.R., Baleg, A.A., Baker, P.G., Iwuoha, E.I., Sensors 10 (**2010**) 9449-65.

Mallakpour, S., Khadem, E., Chem. Eng. J. 302 (**2016**) 344-367.

Manea, F., Motoc, S., Pop, A., Remes, A., Schoonman, J., Nanoscale Res. Lett. 7 (**2012**) 331- 335.

Mehdinia, A., Habib Kazemi, S., Zahra Bathaie, S., Alizadeh, A., Shamsipur, M., Mousavi, M.F., Anal. Biochem. 375 (**2008**) 331–338.

Mehrabi, A., Rahimnejad, M., Mohammadi, M., Pourali, M., Biocatal. Agric. Biotechnol. 22 (**2019**) 101375.

Mekassa, B., Tessema, M., Chandravanshi, B.S., Tefera, M., IEEE Sens. J. 18 (**2018**) 37-44.

Mielech-ŁUkasiewicz, K., Rogińska, K.,. Anal. Methods 6 (**2014**) 7912–7922.

Moghimi, N., Mohapatra, M., Leung, K.T., Anal. Chem. 87 (**2015**) 5546-5552.

Mohamed, A.M.I., Rageh, A.H., Abdel-aal, F.A.M., Ali, A.M.B.H., Electroanalysis 32 (**2020**) 635–647.

Mohammadi, A., Moghaddam, A.B., Alikhani, E., Eilkhanizadeh, K., Mozaffari, S., Micro Nano Lett. 8 (**2013**) 853-857.

Mohanty, U.S., J. Appl. Electrochem. 41 (**2011**) 257-270.

Monk, P.M.S., J. Chem. Educ. 79 (**2002**) 1207.

Montes, R.H.O., Stefano, J.S., Richter, E.M., Munoz, R.A.A., Electroanalysis 26 (**2014**) 1449-1453.

Mostafavi, M., Yaftian, M.R., Piri, F., Shayani-Jam, H., Biosens. Bioelectron. 122 (**2018**) 160-167.

Motoc, S., Remes, A., Pop, A., Manea, F., Schoonman, J., J. Environ. Sci. 25 (**2013**) 838-847.

Mutharani, B., Rajakumaran, R., Chen, S.M., Ranganathan, P., Chen, T.W., Al Farraj, D.A., Ajmal Ali, M., Al-Hemaid, F.M.A., Microchem. J. 159 (**2020**) 105378.

Nair, A.S., Sooraj, M.P., J. Mater. Sci. 55 (**2020**) 3700-3711.

National Center for Health Statistics, 2017. Health, United States, With chartbook on long-term trends in health, Department of Health and Human Services.

Nguyen, N.S., Das, G., Yoon, H.H., Biosens. Bioelectron. 77 (**2016**) 372-7

Nováková, L., Matysová, L., Solich, P., Talanta 68 (**2006**) 908-918.

Oghli, A.H., Soleymanpour, A., Mater. Sci. Eng. C 108 (**2020**) 110407.

Ojani, R., Raoof, J.B., Zamani, S., 2012. Bioelectrochemistry 85 (**2012**) 44–49.

Ottaviano G., Donarelli, M., Sensors 18 (**2018**) 3638.

Patil, S.M., Sataraddi, S.R., Bagoji, A.M., Pathan, R.M., Nandibewoor, S.T., Electroanalysis 26 (**2014**) 831-839.

Paulchamy, B. , Arthi, G., Lignesh, B.D., J. Nanomed. Nanotechnol. 6 (**2015**) 1000253.

Pollap, A., Knihnicki, P., Kuśtrowski, P., Kozak, J., Gołda-Cępa, M., Kotarba, A., Kochana, J., Electroanalysis 30 (**2018**) 2386–2396.

Power, A.C., Gorey, B., Chandra, S., Chapman, J., Nanotechnol. Rev. 7 (**2018**) 19-41.

Pumera, M., 2009. Chem. - A Eur. J. 15 (**2009**) 4970-4978.

Qian, L., Thiruppathi, A.R., Elmahdy, R., van der Zalm, J., Chen, A., Sensors 20 (**2020**) 1252.

Qin, X., Yin, Y., Yu, H., Guo, W., Pei, M.,. Biosens. Bioelectron. 77 (**2016**) 752–758.

Rajaji, U., Manavalan, S., Chen, S.M., Govindasamy, M., Chen, T.W., Maiyalagan, T., Compos. Part B Eng. 161 (**2018**) 29–36.

Rao, C.N.R., Sood, A.K., Subrahmanyam, K.S., Govindaraj, A., Angew. Chemie - Int. Ed. 48 (**2009**) 7752-7777.

Ravat, V., Nongwe, I., Coville, N.J., Microporous Mesoporous Mater. 225 (**2016**) 224-231.

Rocchitta, G., Spanu, A., Babudieri, S., Latte, G., Madeddu, G., Galleri, G., Nuvoli, S., Bagella, P., Demartis, M., Fiore, V., Sensors 16 (**2016**) 780.

Rodríguez, J., Castañeda, G., Lizcano, I.,. Electrochim. Acta 269 (**2018**) 668–675.

Roushani, M., Shahdost-Fard, F., Talanta 144 (**2015**) 510-516.

Ruas De Souza, A.P., Felix, F.S., Castro, P.S., Angnes, L., Bertotti, M., Anal. Methods 8 (**2016**) 1078–1083.

Sanghavi, B.J., Srivastava, A.K., Electrochim. Acta 56 (**2011**) 3731-4424.

Sanghavi, B.J., Srivastava, A.K.,. Analyst 138 (**2013**) 1395-1404.

Sankar, M., Dimitratos, N., Miedziak, P.J., Wells, P.P., Kiely, C.J., Hutchings, G.J., Chem. Soc. Rev. 41 (**2012**) 8099-8139.

Sarhangzadeh, K.,. J. Iran. Chem. Soc. 12 (**2012**) 2133-2140.

Sataraddi, S.R., Patil, S.M., Bagoji, A.M., Pattar, V.P., Nandibewoor, S.T., Anal. Chem. 2014 (**2014**) 9.

Scholz, F., ChemTexts. 4 (**2015**) 17.

Shah, B., Lafleur, T., Chen, A., Faraday Discuss. 164 (**2013**) 135–146.

Shalauddin, M., Akhter, S., Bagheri, S., Abd Karim, M.S., Adib Kadri, N., Basirun, W.J., Int. J. Hydrogen Energy 42 (**2017**) 19951-19960.

Sharafeldin, M., Bishop, G.W., Bhakta, S., El-Sawy, A., Suib, S.L., Rusling, J.F., Biosens. Bioelectron. 91 (**2017**) 359-366.

Shoja, Y., Rafati, A.A., Ghodsi, J., Electrochim. Acta 203 (**2016**) 281-291.

Skrzypek, S., Electroanalysis 22 (**2010**) 2339–2346.

Sousa, T.F.A., Amorim, C.G., Montenegro, M.C.B.S.M., Araújo, A.N., Sensors Actuators B Chem. 176 (**2013**) 660-666.

Stefano, J.S., Montes, R.H.O., Richter, E.M., Muñoz, R.A.A., J. Brazilian Chem. Soc. 25 (**2014**) 484-491.

Su, C., Loh, K.P.,. Acc. Chem. Res. 46 (**2013**) 2275-2285.

Sun, H., Liu, S., Zhou, G., Ang, H.M., Tadé, M.O., Wang, S., ACS Appl. Mater. Interfaces 4 (**2012**) 5466-5471.

Sun, S., Zeng, H. J. Am. Chem. Soc. 124 (**2002**) 8204-8205.

Sun, Y., Xia, Y., Science 298 (**2002**) 2176-2179.

Sundaresan, P., Yamuna, A., Chen, S.M., Ultrason. Sonochem. 67 (**2020**) 105146.

Suresh, E., Sundaram, K., Kavitha, B., Senthil Kumar, N., Int. J. Curr. Pharm. Res. 8 (**2016**) 44-48.

Suryanarayana, C., Mater. Today 8 (**2005**) 62.

Suryanarayanan, V., Zhang, Y., Yoshihara, S., Shirakashi, T., Electroanalysis 17 (**2005**) 925-932.

Švorc, Ľ., Borovská, K., Cinková, K., Stanković, D.M., Planková, A. Electrochim. Acta 251 (**2017**) 621–630.

Taei, M., Hassanpour, F., Salavati, H., Sadeghi, Z., Alvandi, H., Appl. Biochem. Biotechnol. 176 (**2015**) 344–358.

Tajik, S., Safaei, M., Beitollahi, H., Meas. 143 (**2019**) 51-57.

Tajik, S., Taher, M.A., Beitollahi, H., Torkzadeh-Mahani, M., Talanta 134 (**2015**) 60–64.

Tang, Y., Liu, P., Xu, J., Li, L. Le, Yang, L., Liu, X., Liu, S., Zhou, Y., Sensors Actuators B Chem. 258 (**2018**) 906–912.

Tarahomi, S., Rounaghi, G.H., Daneshvar, L., Sensors Actuators B Chem. 286 (**2019**) 445-450.

Tashkhourian, J., Hemmateenejad, B., Beigizadeh, H., Hosseini-Sarvari, M., Razmi, Z., J. Electroanal. Chem. 715 **(2014**) 103-108.

Teymourian, H., Salimi, A., Khezrian, S.,. Biosens. Bioelectron. 49 (**2013**) 1-8.

Ting, B.P., Zhang, J., Gao, Z., Ying, J.Y., Biosens. Bioelectron. 25 (**2009**) 282–287.

Todakar, A., Shetti, N.P., Devarushi, U.S., Tuwar, S.M.,. Mater. Today Proc. 18 (**2019**) 550–557.

Tseng, T.W., Rajaji, U., Chen, T.W., Chen, S.M., Huang, Y.C., Mani, V., Irudaya Jothi, A., Ultrason. Sonochem. 69 (**2020**) 105242.

Devarushi U., Shetti N, Tuwar S., Seetharamappa J., Anal. Bioanal. Chem. 9 (**2017**) 102–116.

Uslu, B., Doğan, B., Özkan, S.A., Anal. Chim. Acta 537 (**2005**) 307–313.

Uzun, L., Turner, A.P.F., Biosens. Bioelectron. 76 (**2016**) 131-144.

Vane, J.R., Botting, R.M., Am. J. Med 104 (**1998**) 2-8.

Verma, H.N., Singh, P., Chavan, R.M., Vet. World 7 (**2014**) 72-77.

Wackerlig, J., Lieberzeit, P.A., Sensors Actuators B Chem. 207 (**2015**) 144-157.

Wahyuni, W.T., Ivandini, T.A., Jiwanti, P.K., Saepudin, E., Gunlazuardi, J., Einaga, Y., Electrochemistry 83 (**2015**) 357–362.

Wang, F., Chen, L., Chen, X., Hu, S., St, Anal. Chim. Acta 576 (**2006**) 17–22.

Wang, H., Zhao, H., Quan, X., Chen, S., Electroanalysis 23 (**2011**) 1863–1869.

Wang, P., Gan, T., Zhang, J., Luo, J., Zhang, S., J. Mol. Liq. 177 (**2013**) 129–132.

Wei, S., Liu, Y., Hua, T., Liu, L., Wang, H., J. Appl. Polym. Sci. 131 (**2014**) 4–11.

White, R.J., Luque, R., Budarin, V.L., Clark, J.H., Macquarrie, D.J., Chem. Soc. Rev. 38 (**2009**) 481-494.

Wolfender, J.L.,Planta. Med. 75 **(2009)** 719-734

Wong, A., Santos, A.M., Cincotto, F.H., Moraes, F.C., Fatibello-Filho, O., Sotomayor, M.D.P.T., Talanta 206 (**2020**) 120252.

Wong, Y.C., Ang, B.C., Haseeb, A.S.M.A., Baharuddin, A.A., Wong, Y.H., J. Electrochem. 167 (**2019**) 037503.

Wu, G., Wang, X., Guan, N., Li, L., Appl. Catal. B Environ. 137 (**2013**) 177-185.

Wu, T., Li, T., Liu, Z., Guo, Y., Dong, C., Talanta 164 (**2017**) 556–562.

Xu, X., Zhou, G., Li, H., Liu, Q., Zhang, S., Kong, J., Talanta 78 (**2009**) 29-32.

Yamuna, A., Sundaresan, P., Chen, S.M., Ultrason. Sonochem. 64 (**2020**) 105014.

Yang, C., Denno, M.E., Pyakurel, P., Venton, B.J., Anal. Chim. Acta 887 (**2015**) 17-37.

Yang, J., Wang, P., Zhang, X., Wu, K., J. Agric. Food Chem. 57 (**2009**) 9403–9407.

Yang, X., Yu, X., Heng, Y., Wang, F., J. Electroanal. Chem. 816 (**2018**) 54–61.

Yao, Y., Jiang, C., Ping, J., Biosens. Bioelectron. 123 (**2019**) 178–184.

Yari, A., Shams, A., Electroanalysis 30 (2**018**) 803–809.

Yashin, Y.I., Yashin, A.Y., Walton, H.F., 2004. 2nd Ed. Elsevier, Amsterdam, Netherlands.

Ye, Z., Yang, L., Wen, J., Ye, B., Anal. Methods 7 (**2015**) 2855–2861.

Yi, W., Li, Z., Dong, C., Li, H.W., Li, J., Microchem. J. 148 (**2019**) 774–783.

Yiğit, A., Yardim, Y., Şentürk, Z., IEEE Sens. J. 16 (**2016**) 1674-1680.

Yin, J., Guo, W., Qin, X., Zhao, J., Pei, M., Ding, F., Sensors Actuators B Chem. 241 (**2017**) 151–159.

Yola, M.L., Atar, N., Eren, T., Karimi-Maleh, H., Wang, S., RSC Adv. 5 (**2015**) 65953–65962.

Yousefi, A., Babaei, A., Delavar, M., J. Electroanal. Chem. 822 (**2018**) 1–9.

Zad, Z.R., Davarani, S.S.H., Taheri, A., Bide, Y., J. Mol. Liq. 253 (**2018**) 233–240.

Zhang, Y., Cheng, W., Li, S., Li, N., Colloids Surfaces A Physicochem. Eng. Asp. 286 (**2006**) 33–38.

Zhao, J., Guo, W., Pei, M., Ding, F., Anal. Methods 8 (**2016**) 4391–4397.

Zheng, J., Zhang, M., Ling, Y., Xu, J., Hu, S., Hayat, T., Alharbi, N.S., Yang, F., J. Electroanal. Chem. 818 **(2018**) 97–105.

Zhou, L., Li, D.J., Gai, L., Wang, J.P., Li, Y. Bin, Sensors Actuators B Chem. 162 (**2012**) 201–208.

Zhou, M., Zhai, Y., Dong, S., Anal. Chem. 81 **(2009**) 5603-13.

Zhou, Y., Zhi, J., Zhang, X., Xu, M., 2011. Diam. Relat. Mater. 20 (**2011**) 18–22.

Scheme and Figures

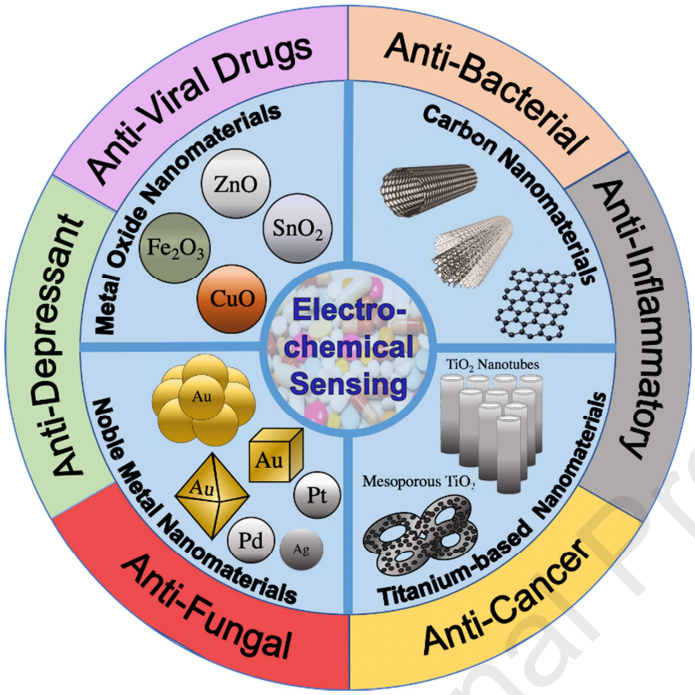

Scheme 1. Illustration of nanomaterials employed as electrochemical catalyst for the detection for the detection of pharmaceutical compounds.

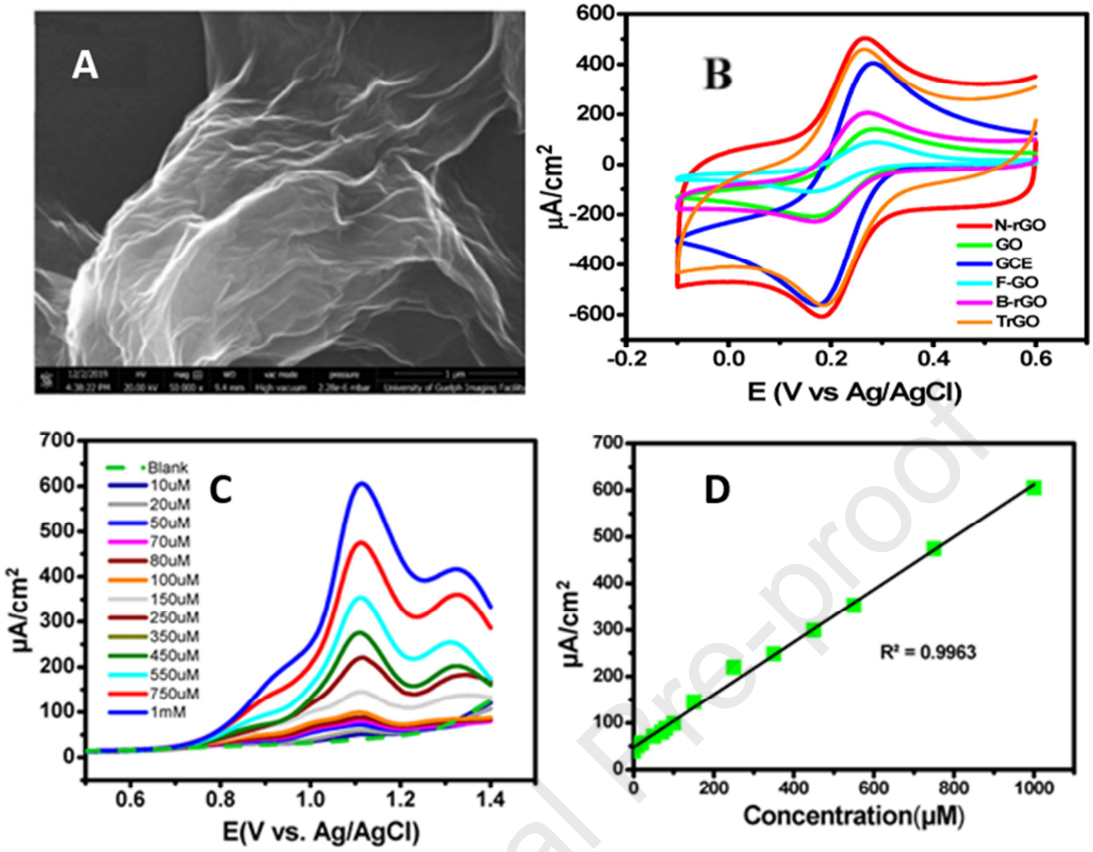

Figure 1. (A) SEM image of graphene oxide at 50,000X magnification; (B) CV scans of multiple of various graphene oxide-based electrodes recorded in (5 mM $K_3[Fe(CN)_6]$ in 0.2 M KNO_3 at a scan rate of 50 mV s^{-1} (N-rGO: nitrogen doped reduced graphene oxide; GO: graphene oxide; GCE: glassy carbon electrode; F-GO: fluorine doped graphene oxide; B-rGO: boron doped reduced graphene oxide; TrGO: thermally reduced graphene oxide). (C) DPV curves recorded at different naproxen concentrations in 0.1 M PBS buffer solution with GO/GCE; (D) Calibration curve of increasing naproxen concentration ranging from 10 µM to 1 mM (Qian et al, **2020**).

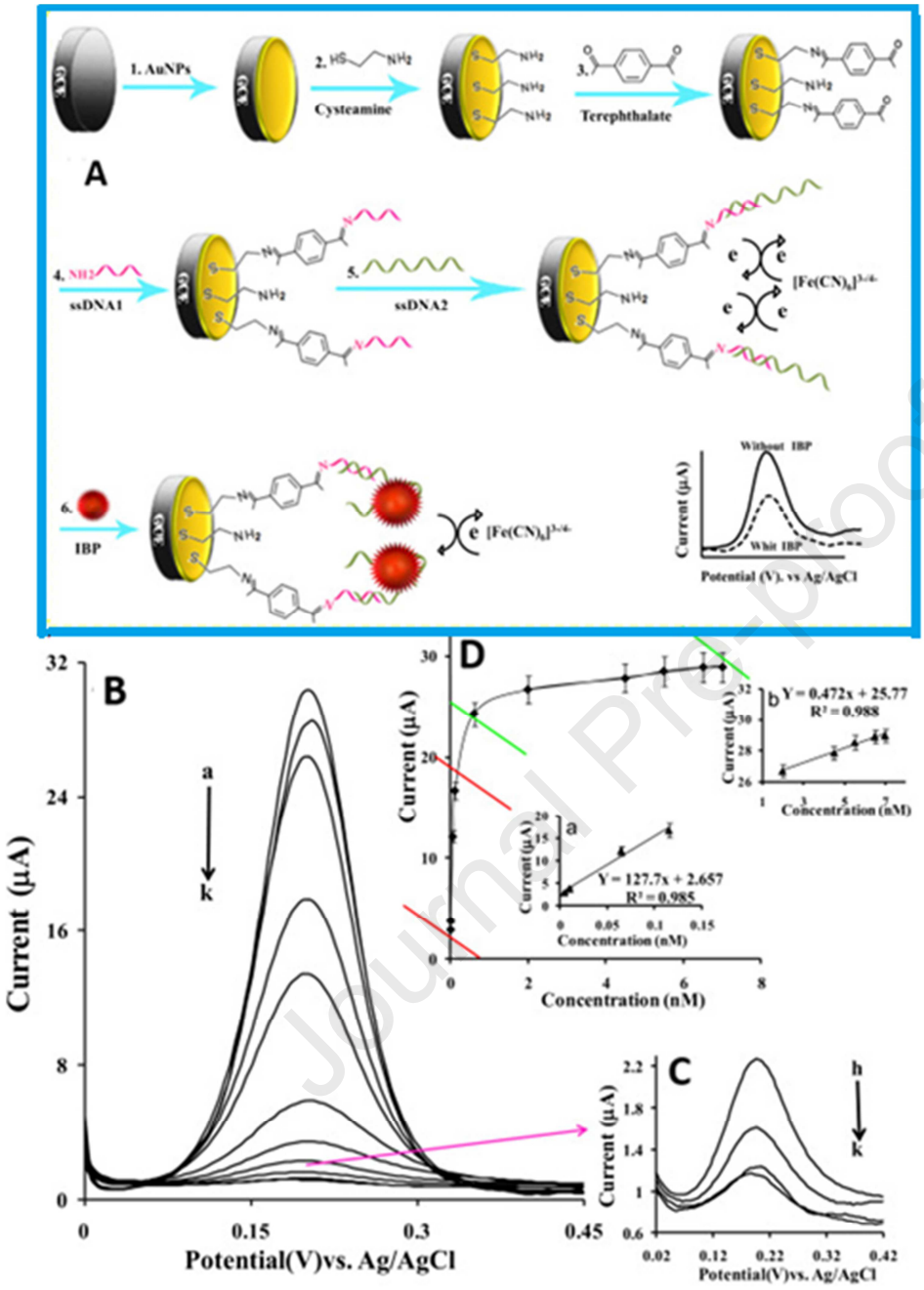

Figure 2. (A) Fabrication process of the aptamer and gold nanoparticles functionalized GCE; (B) DPV curves of the developed nanoaptasensor in the presence of different ibuprofen concentrations of 0, 0.005, 0.01, 0.065, 0.115, 2, 4.5, 5.5, 6.5, 7 nM (from top to bottom) record in $[Fe(CN)_6]^{3-/4-}$ as the electrolyte solution; (C) Magnified curves; (D) Calibration curve of DPV response vs concentrations in two ranges (a and b) (Roushani and Shahdost-Fard, **2015**).

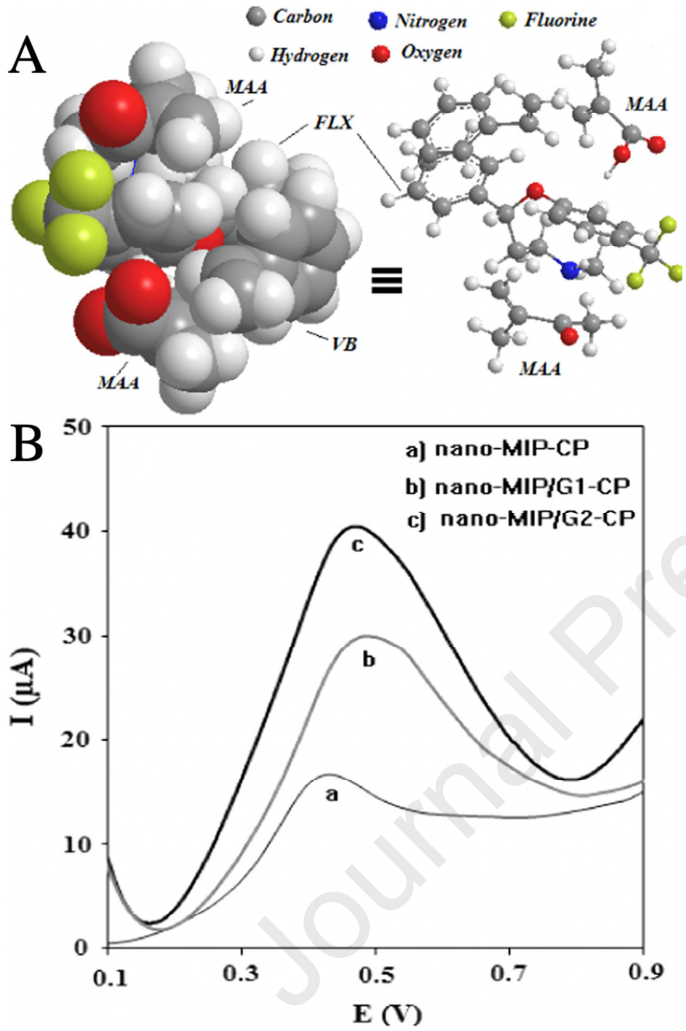

Figure 3. (A) Optimized conformation of self-assembly complex of fluoxetine and functional monomers (MAA: methacrylic acid; VB: vinyl benezenel; FLX: fluoxetine); (B) Comparison of DPV plots of different molecular-inprinted polymer modified carbon paste (nano-MIP-CP) electrodes (Alizadeh and Azizi, **2016**).

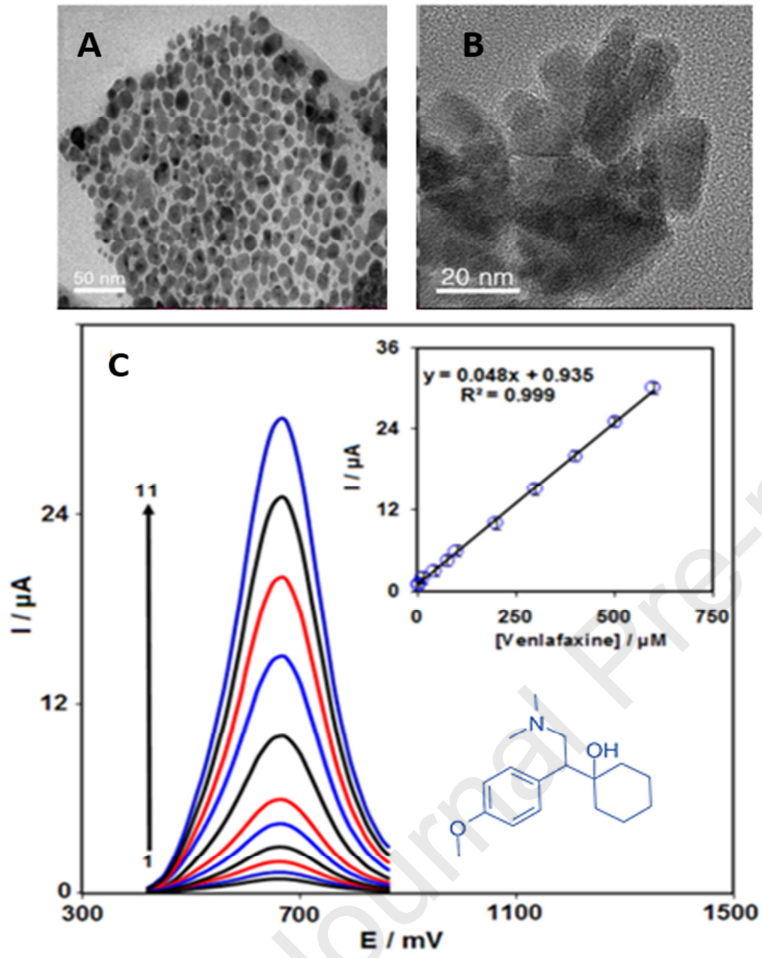

Figure 4. (A) and (B) High-resolution transmission electron microscopy (HRTEM) images of Fe_3O_4@CNC/Cu catalyst; (C) DPVs of Fe_3O_4@CNC/Cu/GSPE in 0.1 M PBS (pH 7.0) containing increasing concentration of venlafaxine (insert: the associated calibration curve with venlafaxine concentration ranging from 0.05 to 600 µM) ((Khalilzadeh et al., **2020)**.

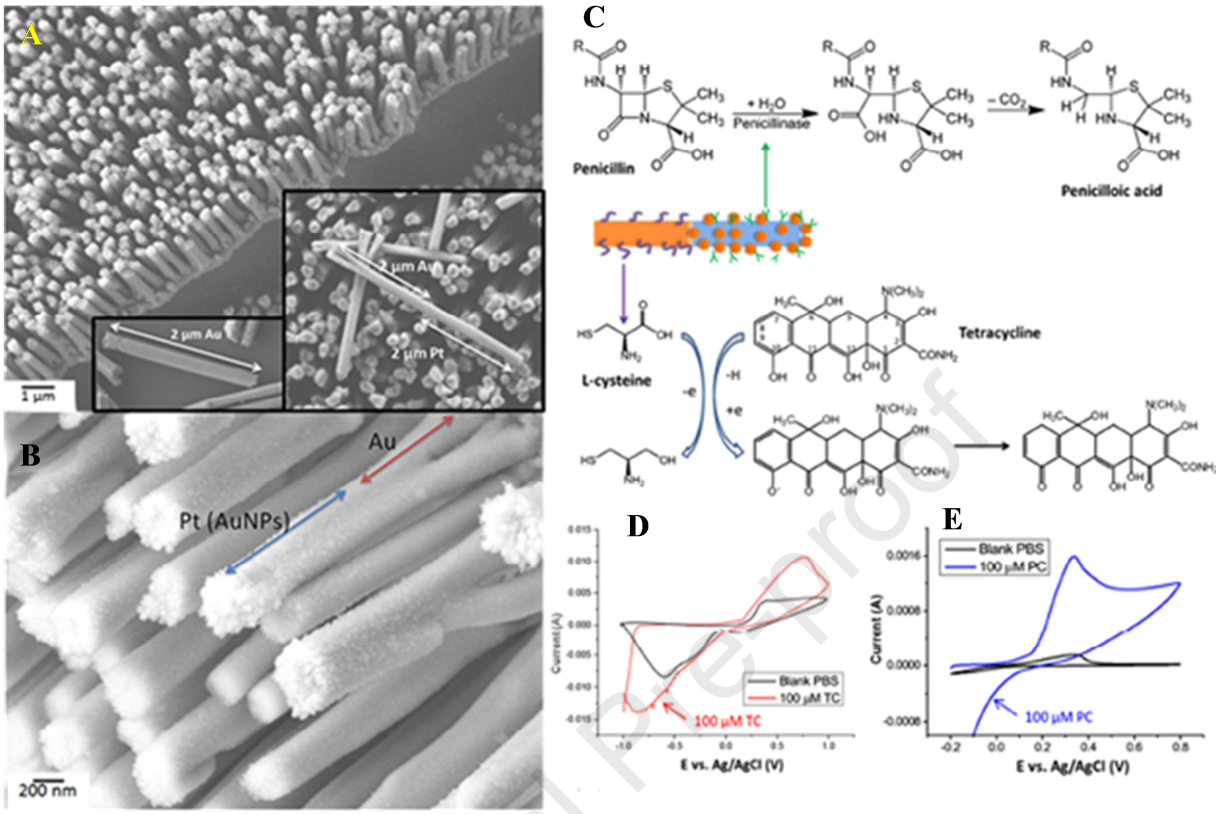

Figure 5. (A) FE-SEM images of Au-Pt multisegmented nanowire array and single Au nanowire and single Au-Pt nanowire; (B) AuNPs coated on Pt segment after being treated by 3 mM $HAuCl_4$ solution; (C) The sensing mechanism of penicillinase with penicillin; L-cysteine with tetracycline; (D) CV scan of Au(L-cysteine) nanowire array sensing 100 μM tetracycline and (E) penicillin in 1 mM PBS buffer solution (E) (Li et al., **2019**).

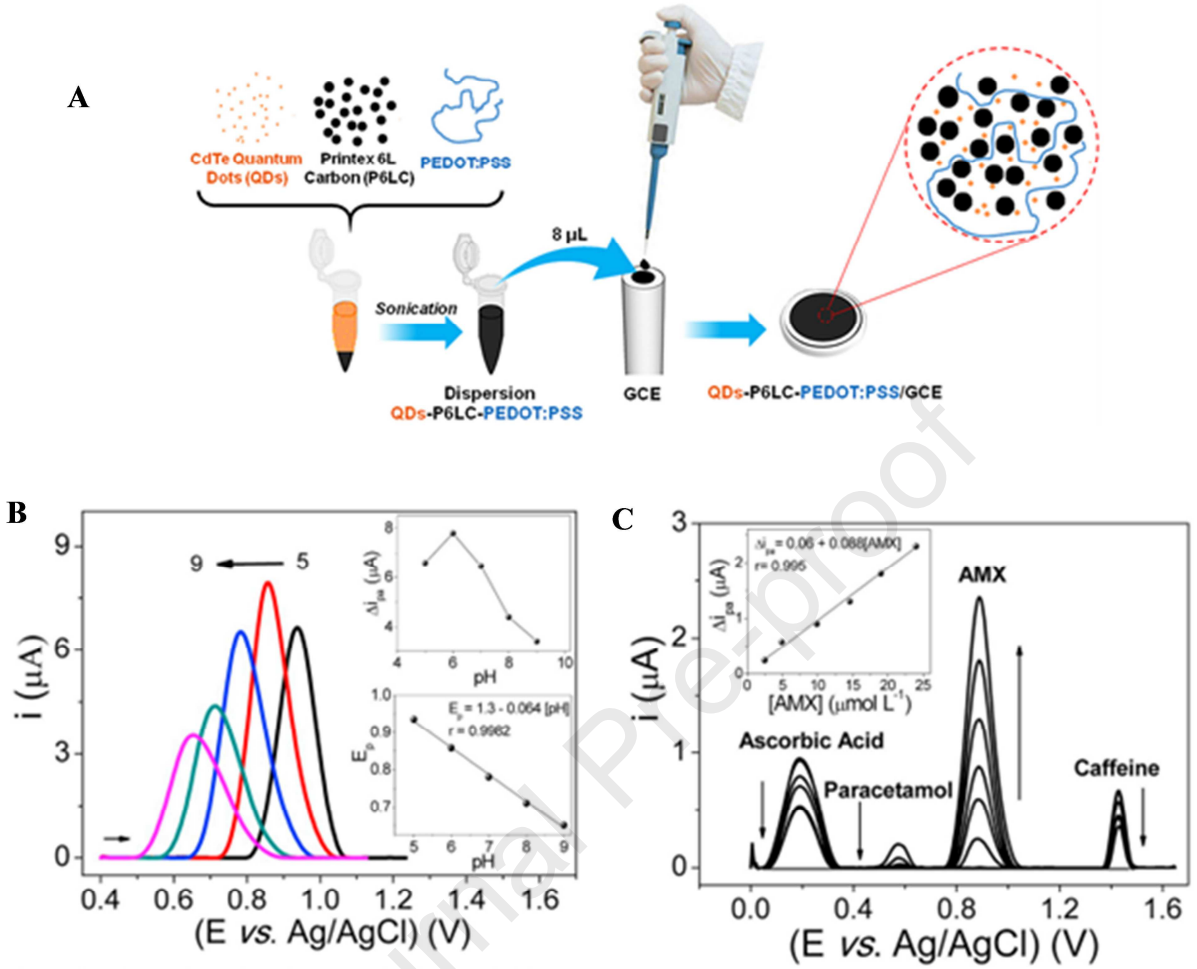

Figure 6. (A) Representation of preparation of quantum dots-based sensor; (B) Effect of pH on the anodic peak current and peak potential of the QDsP6LC-PEDOT:PSS/GCE sensor in 0.1 M phosphate buffer solution; (C) Determination by SWV of AMX in presence of ascorbic acid and caffeine. Analysis conditions: AMX at different concentrations (in a range of 0.90 – 24 µM), 20 µM ascorbic acid. 20 µM paracetamol and 10 µM caffeine in 0.1 M phosphate buffer solution (pH 6.0) (A. Wong et al., **2020**).

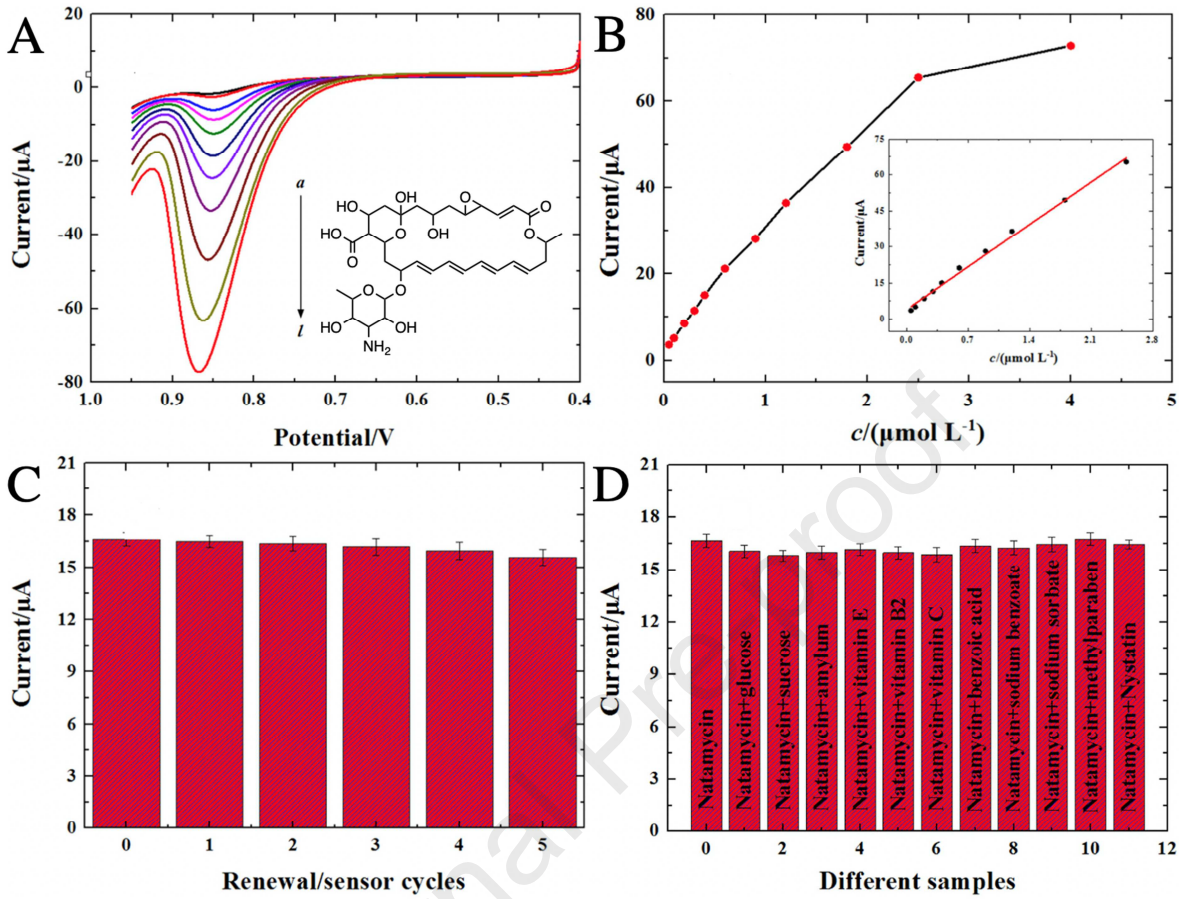

Figure 7. (A) The response of different concentration of natamycin by linear sweep adsorptive stripping voltammetry; (B) Relationship of *c* for *i*pa, the inset shows corresponding calibration curve; (C) Influence of renewal step on the *i*pa detected at 3DG-MWCNT/GCE; (D) Influence of different interfering compounds on the *i*pa detected at 3DG-MWCNT/GCE (Yang et al., **2018**).

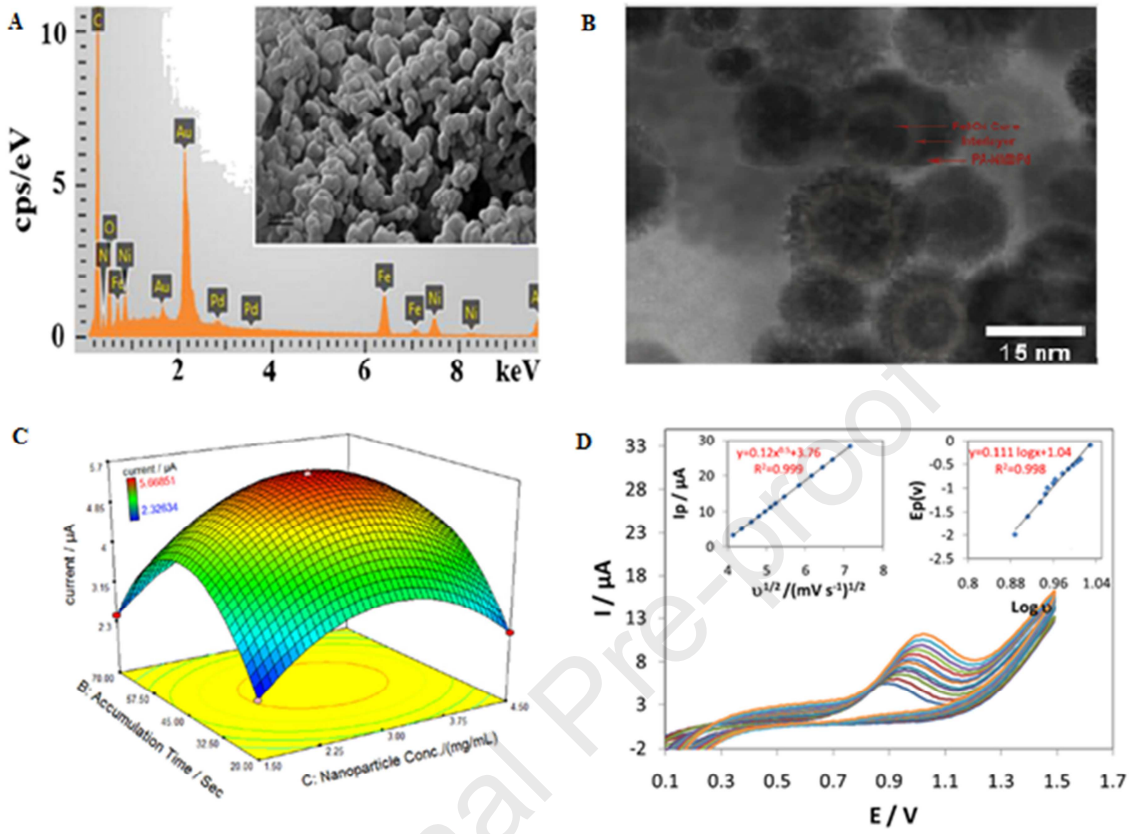

Figure 8. (A) X-ray photoelectron spectrum of yolk–shell Fe_3O_4@PA-Ni@Pd (Inset: the corresponding EDS); (B) TEM image of the yolk–shell Fe_3O_4@PA-Ni@Pd; (C) Effect of the accumulation time and the concentration of the 3D response surface of the modified electrochemical sensor to FLU; (D) CV of FLU at different scan rates from 10 to 500 mV s^{-1} (Inset: dependence of peak current value on scan rate and dependence of Ep value on υ (Yang et al., **2020**).

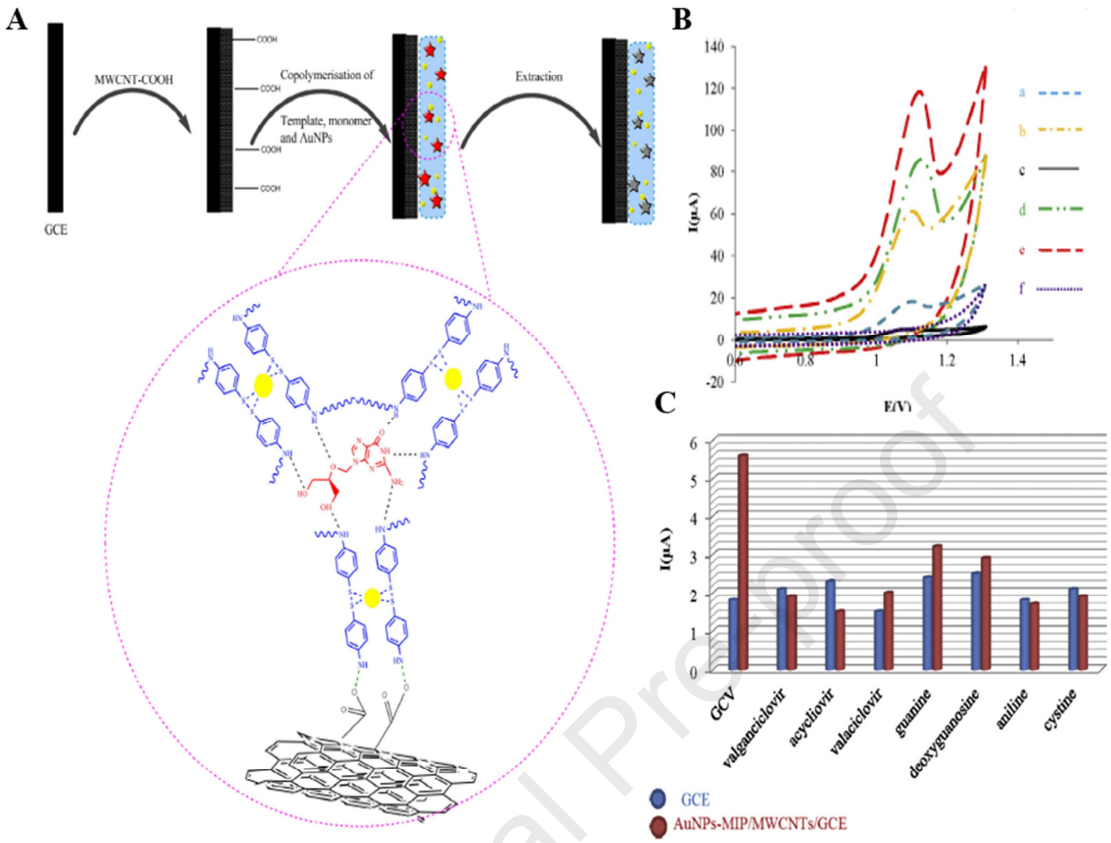

Figure 9. (A) Scheme of the fabrication of molecularly imprinted polymer structure; (B) CVs of phosphate buffer solution (pH 3) containing 100 μM GCV at (a) GCE; (b) MWCNT/GCE; (NIP/MWCNT/GC, (d) MIP/MWCNT/GCE, (e) AuNPs/MIP/MWCNT/GCE and (f) AuNPs/MIP/MWCNT/GCE in phosphate buffer solution, Scan rate = 100 mV s^{-1}; (C) Responses of AuNPs/MIP/MWCNT/GCE and GCE immersed in the solutions containing 100 μM of each drug (Gholivand and Karimian, **2015**).

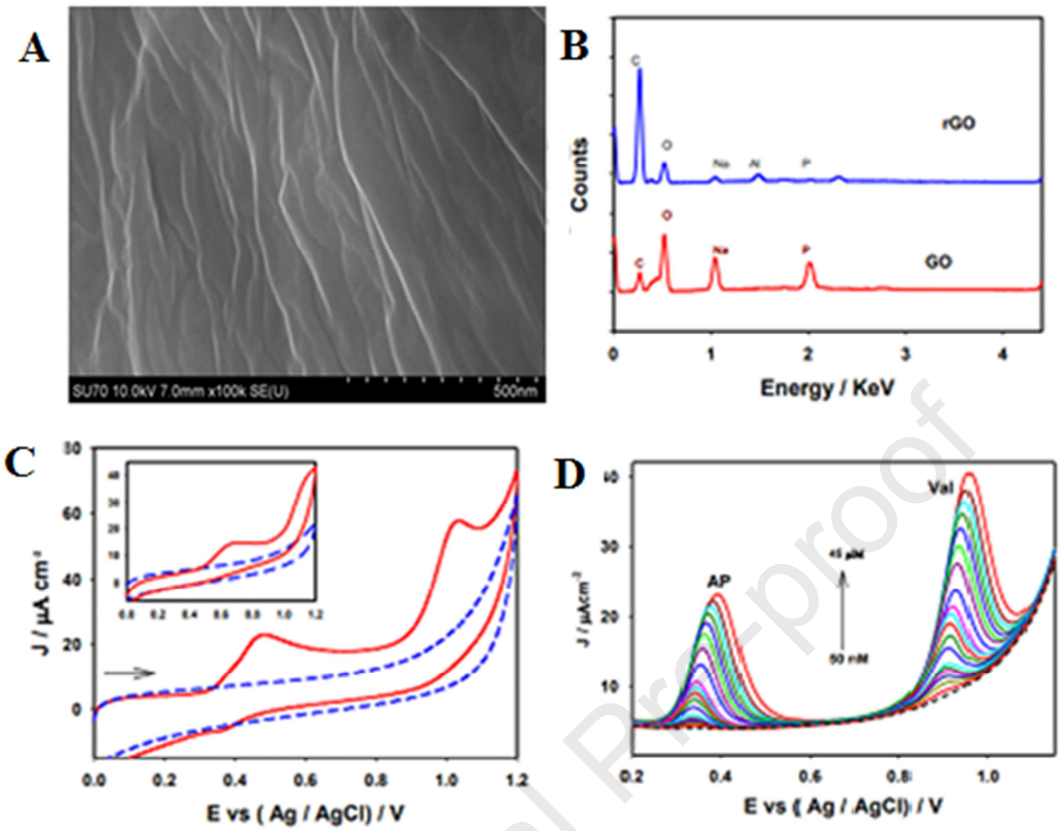

Figure 10. (A) □E□ im□□□of GCE followi□□modifi□□tio□with □l□□tro□h□mi□□lly rGO (rGO); (B) EDX □p□□trum of rGO □□d GO film o□ th□ □l□□trod□ □urf□□□; (C) CV □urv□□ of □mixtur□ of □□□t□mi□oph□□ □□d v□l□□y□lovir □olutio□ □t th□ rGO/GCE (I□□□rt: GCE); (D) R□□po□□□□ of th□ rGO/GCE to th□ □u□□□□iv□ □dditio□ of both □□□t□mi□oph□□ □□d v□l□□y□lovir i□ 0.1 □ PB□ (pH 7.2) (C & D) (Adhik□ri □t □l, **2016**).

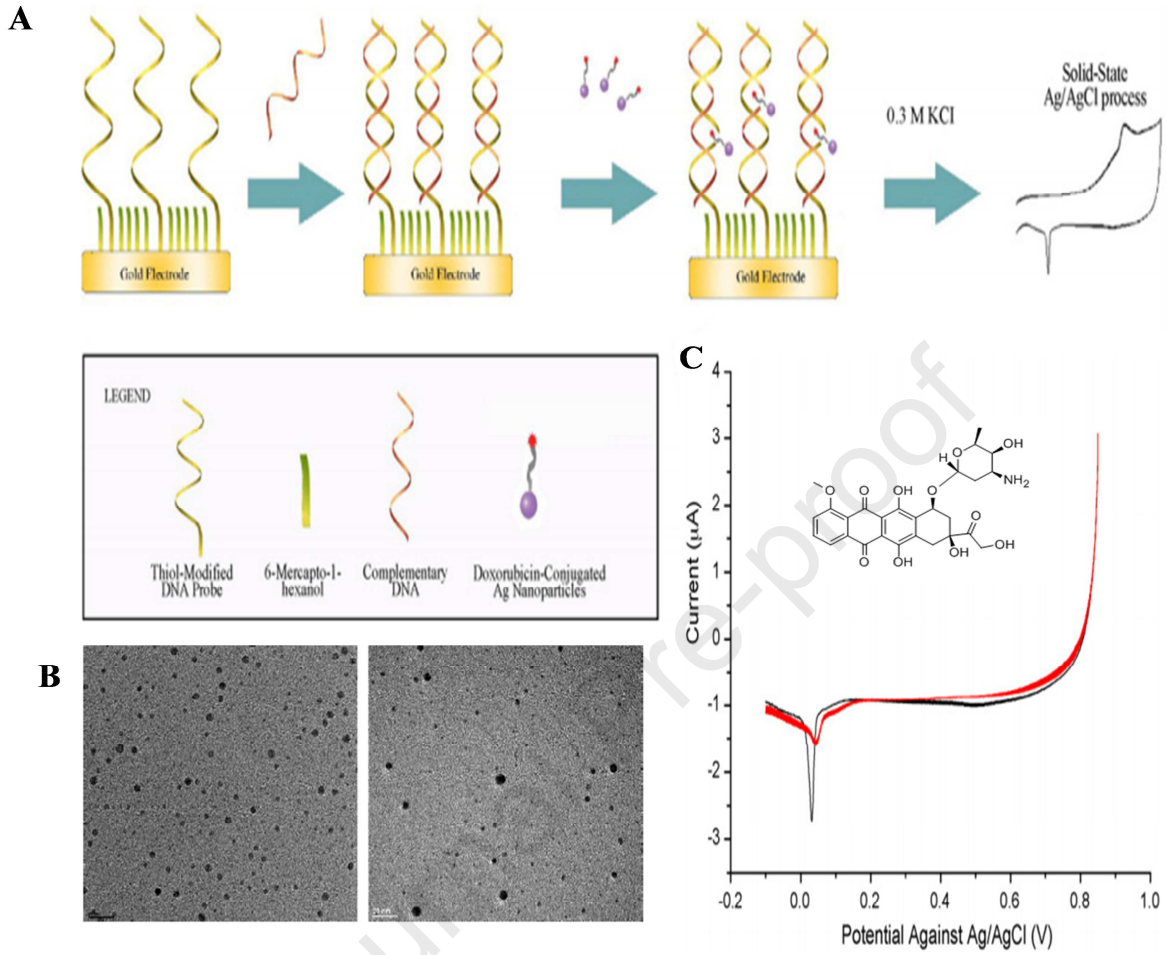

Figure 11. (A) Schematic representation of DNA sensor development; (B) TEM images of Ag nanoparticles (a) before and (b) after conjugation with doxorubicin. Scale bar = 20 nm; (C) Comparison of voltammetric results measured in 0.3 M of KCl when a doxorubicin loading per Ag nanoparticle of (red line) ~17 and (black line) ~1 was used in the labeling process (Ting et al., **2009**).

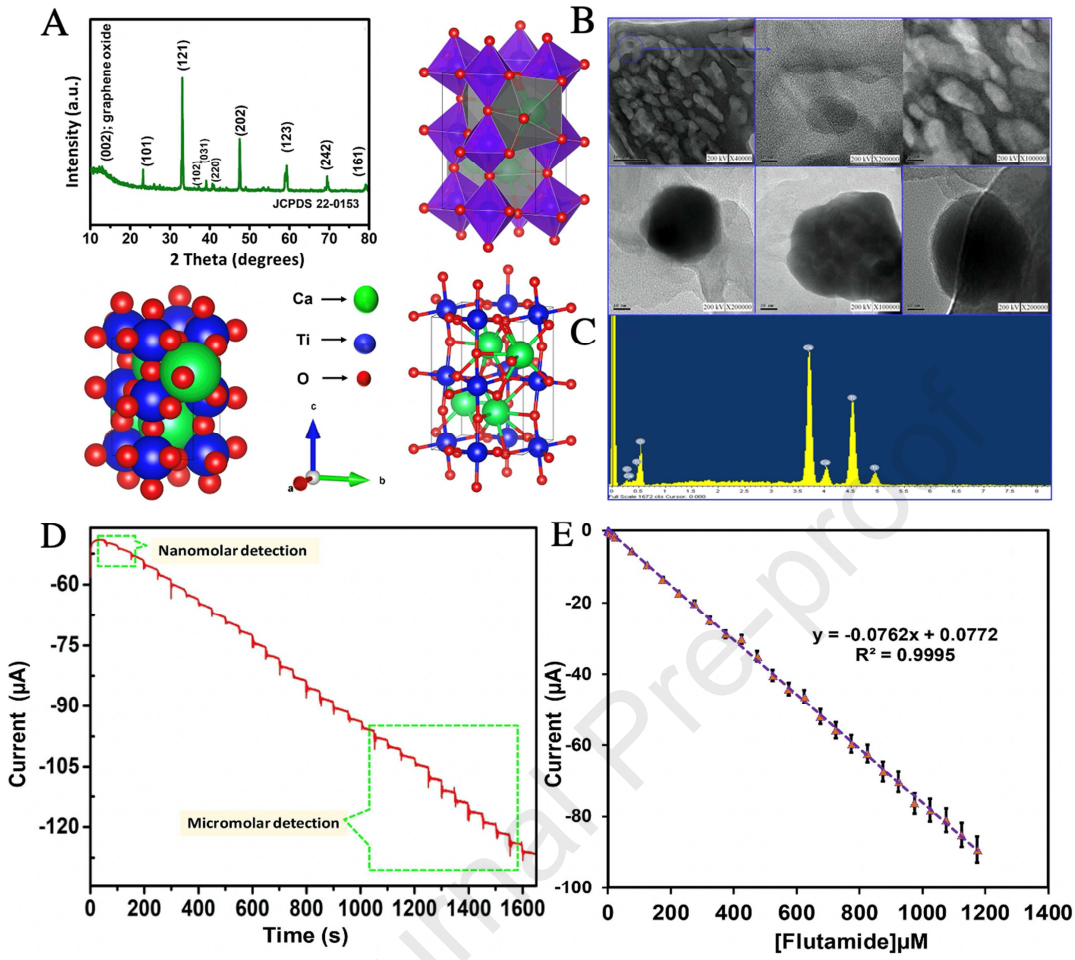

Figure 12. (A) XRD analysis of GOS/$CaTiO_3$ nanocomposite (JCPDS number: 22-0153) and the crystal structures of the nanocomposite's orthorhombic structure; (B) TEM images of GOS/$CaTiO_3$ nanomaterial; (C) EDS analysis of GOS/$CaTiO_3$ nanocomposite; (D) i-t responses for the low and high concentrations of flutamide drug in 0.05 M phosphate buffer (pH 7.0) at GOS/$CaTiO_3$ modified GCE (RPM = 1200); (E) The linear plot of [flutamide] (µM) versus cathodic peak currents (Tseng et al., **2020**).

Table. 1. A list of advanced nanomaterials-based electrochemical sensor and biosensor platforms for the detection of pharmaceutical compounds

Pharmaceutical Compound	Electrode	Method	Medium/Sample	Linear Range	LOD	Reference
Naproxen 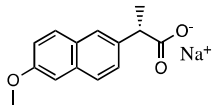	BDDE	DPV	0.1 M $LiClO_4$	0.5 – 50.0 µM	30.0 nM	Suryanarayanan et al., **2005**
	GCE	DPV	0.1 M PBS pH 7	10.0 – 125.0 µM	0.3 µM	Stefano et al., **2014**
	NiO-CNT-IL/CPE	SWV	0.1 M PBS pH 7	0.75 – 800.0 µM	0.12 µM	Beitollahi and Yoonesfar, **2016**
	AgNPs-GO-B-CD/G-DVD	DPV	0.1 M PBS pH 7	0.4 – 80 µM	23.0 nM	Tarahomi et al., **2019**
	ZnO/MWCNT/CPE	SWV	0.1 M PBS pH 7	1.0 – 200 µM	0.23 µM	Tashkhourian et al., **2014**
	MWCNT/GCE	CA	PBS pH 7	10.0 – 200.0 µM	0.6 µM	Montes et al., **2014**
	MWCNT-Gr-IL/CCE	DPV	PBS pH 7	0.8 – 100.0 µM	0.13 µM	Sarhangzadeh, **2015**
Ibuprofen 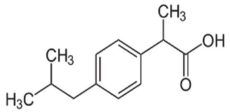	CPE	DPV	PBS pH 7	0.1 – 100.0 µM	0.1 µM	Brycht et al., **2015**
	BDDE	DPV	0.1 M H_2SO_4	20.0 – 1000.0 µM	5.0 µM	Lima et al., **2013**
	AgZCNF	DPV	0.1 M Na_2SO_4	0.5 – 5.0 ppm	0.008 ppm	Manea et al., **2012**
	CD-PS	Potentiometry	NH_3 buffer pH 9	3.9 – 1000.0 µM	3.34 µM	Sousa et al., **2013**
	Cu_3TeO_6/GCE	DPV	0.1 M ABS pH 4.7	0.02 – 5.0 µM	0.017 µM	Mutharani et al., **2020**
	Pretreated SPGE	SWV	0.25 M ABS pH 4.7	–	1.3 µg cm^{-3}	Amin et al., **2014**
	AgZMWCNT	DPV	0.1 M Na_2SO_4	9.7 – 48.4 µM	0.082 µM	Motoc et al., **2013**
	PANI-NF/GCE	DPV	Ethanol	0.2 – 0.4 µM	0.1 µM	Suresh et al., **2016**
	P(L-ASP)/GCE	SWV	0.25 M ABS	1.0 – 150.0 µM	0.22 µM	Mekassa et al., **2018**
Aspirin 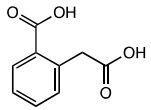	Graphene	DPV	0.2 M PBS pH 7	1.0 – 200.0 µM	0.02 µM	Patil et al., **2014**
	MIP/SiO_2@Au	DPV	0.1 M PBS pH 7	0.001 – 0.01 µM	0.000sd2 µM	Deiminiat et al., **2017**
	BDDE	DPV	0.1 M PBS pH 2.5	5.0 – 125.0 ppm	1.310 ppm	Yiğit et al., **2016**
Diclofenac 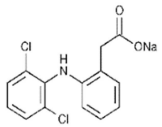	Polyaniline/rGO	DPV	0.1 M $HClO_4$	5.0 – 30.0 ppm	1.1 ppm	Mostafavi et al., **2018**
	Cu/CTS/MWCNT/GCE	SWV	0.1 M PBS pH 4	0.3 – 200 µM	21.0 nM	Shalauddin et al., **2017**
Fluoxetine 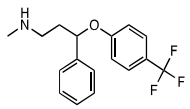	BDDE	DPV	PBS pH 7	0.1 – 0.9 µM	7.0 nM	Brycht et al., **2015**
	Graphite/MIP CP	DPV	Buffer pH 10	0.006 – 10 µM	3.0 nM	Alizadeh and Azizi, **2016**
	CNPs/GCE	DPV	Acetonitrile pH 9	1 – 25 µM	0.4 µM	Mohammadi et al., **2013**
Paroxetine 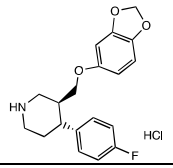	rGO/PWA/PGE	DPV	Borate buffer pH 7	0.008 – 1 µM	0.9 nM	Oghli and Soleymanpour, **2020**
	BDDE	DPV	PBS pH 7	0.1 – 0.9 µM	0.38 µM	Brycht et al., **2015**
Sertraline	Ni (II)-LD/AuNP.MWCNT	DPV	0.1 M NaOH	0.05 – 5.5 µM	95.0 nM	Shoja et al., **2016**
	MIP/Gr-SPCE	DPV	B.R. buffer pH 7	0.005 – 0.08 µM	0.002 µM	Khosrokhavar et al., **2020**

Pharmaceutical Compound	Electrode	Method	Medium/Sample	Linear Range	LOD	Reference
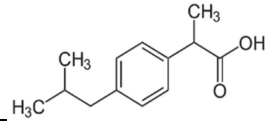	$ZnFe_2O_4$/SPE	DPV	0.1 M PBS pH 7	0.07 – 300.0 µM	0.02 µM	Tajik et al., **2019**
Venlafaxine 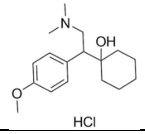	Fe_3O_4@CNC/Cu	DPV	0.1 M PBS pH 7	0.05 – 600.0 µM	0.01 µM	Khalilzadeh et al., **2020**
	NAF-CNT-GCE	AdsDPV	NH_3 buffer pH 9	3.87 – 10000.0 µM	3.34 µM	Sanghavi and Srivastava, **2011**
Imipramine 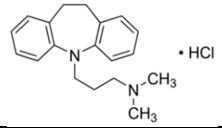	DNA-GP	DPV	0.17 M PBS pH 7.5	0.005 – 0.05 µM	0.5 nM	Jankowska-Śliwińska et al., **2015**
	MIP/Au-NP/ITO	DPV	0.1 M PBS pH 2.3	5.0 – 1000.0 µM	1.0 nM	Xu et al., **2009**
	XAD2-TNP-GCPE	AdsDPV	0.1 M PBS pH 6	0.0013 – 6.2 µM	0.9 nM	Sanghavi and Srivastava, **2013**
Desipramine 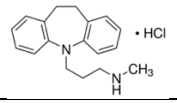	XAD2-TNP-GCPE	AdsDPV	0.1 M PBS pH 6	0.0014 – 6.9 µM	0.4 nM	Sanghavi and Srivastava, **2013**
	BDDE	DPV	0.1 M PBS pH 6.9	0.01 – 100.0 µM	0.01 µM	Ivandini et al., **2002**
Amoxicillin 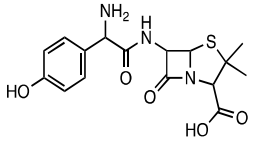	TiO_2/CMK/AuNPs/Nafion/ GCE	CV	Milk samples	2.5 – 133.0 µM	0.3 µM	Pollap et al., **2018**
	CB/DPH/GCE	SWV	Milk samples	2.0 – 18.8 µM	0.1 µM	Deroco et al., **2018**
	AuNPs/PdNPs/ErGO/GCE	SWV	Milk samples	30.0 – 350.0 µM	9.0 µM	Kumar et al., **2011**
	Ni/CR/CPEs	Amperometry	Milk samples	8.0 – 100.0 µM	5.0 µM	Ojani et al., **2012**
	QDs-P6LC-PEDOT:PSS/GCE	SWV	Milk samples	0.90 – 69 µM	50 nM	A. Wong et al., **2020**
Streptomycin 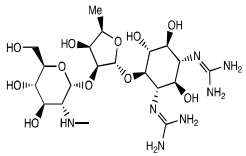	(Apt)-CS conjugate/gold electrode	CV, DPV	Human serum	30 – 1500 nM	15.3 nM	Danesh et al., **2016**
	RuO_2-modified CPEs	Amperometry	Pharmaceutical products	1.5 – 250 µM	1.5 nM	Leech et al., **1990**
	GR–Fe_3O_4–AuNPs	CV, EIS, DPV	Milk	0.05 – 200 µg L^{-1}	0.028 µg L^{-1}	Yin et al., **2017**
	TRSiN/GCE	DPV	Honey, peanut, milk. Porcine kidney and muscle	0.05 – 50 µg L^{-1}	5.0 ng L^{-1}	Liu et al., **2011**
	mMip- GOX-STR	SWV	Milk and honey	0.05 – 20 µg L^{-1}	10.0 ng L^{-1}	Liu et al., **2013**
Ampicillin 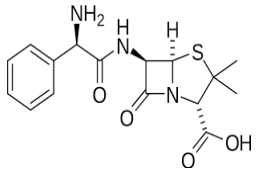	rGO/SPCE	CV	0.1 M H_2SO_4	1 – 50 µmol	0.12 µM	Latif and Merza, **2016**
	SD-EAS II	SWV		1 nM – 1 mM	1.0 nM	Yang., **2019**
	Pt-CdS/MWCNT/SPCE	DPV	0.1 M H_2SO_4	0.2 – 70.0 µM	0.12 µM	Wei et al., **2014**
	Co-MOF-on-TPN-COF	EIS	Human serum, milk, river water	1.0 pg L^{-1} – 2.0 µg L^{-1}	0.217 pg L^{-1}	Liu et al., **2019**
Tetracycline	Anti-TET/MWCNT/GCE	DPV	Spiked milk sample	0.01 – 50 µM	5.0 nM	Zhou et al., **2012**

Pharmaceutical Compound		Electrode	Method	Medium/Sample	Linear Range	LOD	Reference
	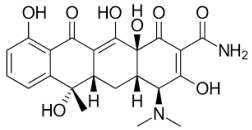	MWCNT-GNPs/MIP/GCE	CV		0.22 – 90 µM	90.0 nM	Wang et al., **2011**
		MB/Anti-TET/AuNps/GCE	CV	Milk sample	0.1 nM – 1 mM	4.0 pM	Guo et al., **2015**
		Au colloids/ME	CV	PBS	2.3 – 22.5 µM	0.2 µM	Wang et al., **2012**
		PtNPs/c/GCE	DPV	Human urine sample	9.9 – 44.01 µM	4.3 µM	Kushikawa et al., **2016**
Triclosan	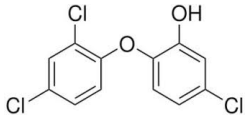	MWCNT	CV, DPV	Toothpaste	0.050 – 1.75 mg L^{-1}	16.5 µg L^{-1}	Yang et al., **2009**
		CNDs/GCE	CV, EIS	Toothpaste	10 nM – 1.0 mM	9.2 nM	Dai et al., **2012**
		CNT/Fe_3O_4@PPy/Pd	DPV	Toothpaste	2.247 – 275.2 nM	1.4 nM	Zheng et al., **2018**
		PDDA-Gr/PdNPs	DPV	Tap water samples	9.00 – 20,000 nM	3.5 nM	Wu et al., **2017**
		AuNPs/POM/rGO/GCE	CV, EIS	Wastewater and lake water	0.5 – 50.0 nM	0.15 nM	Yola et al., **2015**
Ciclopirox olamine	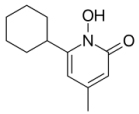	Au-In_2O_3-CS/ABPE	CV, SWV	PBS pH 7	0.199 – 16.22 µM	6.6 nM	H. Ibrahim et al., **2018**
		GCE	Amperometry	Pharmaceutical drug	2.0 – 200 mM	1.0 mM	Ferreira et al., **2012**
		Boron-doped electrode	CV, SWV	Water	25.3 – 419 µM	6.7 µM	Mielech-ŁUkasiewicz and Rogińska, **2014**
		Gold microarray electrode	Amperometry	Pharmaceutical drug	60 – 1100 µM	3.0 µM	Ruas De Souza et al., **2016**
Natamycin	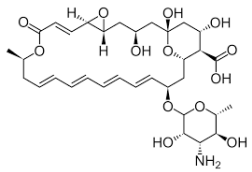	CPE	DPV		2.0 – 80 µM	1.5 µM	Aki et al., **2005**
		SWNT/poly(L-serine)/GCE	LSASV	0.2 M ABS	0.06 – 6.0 µM	40.0 nM	Ye et al., **2015**
		3DG-MWCNT/GCE	LSASV		0.050 – 2.5 µM	10.0 nM	Yang et al., **2018**
		Pt-CdS/MWCNT/SPCE	DPV	0.1 M H_2SO_4	0.2 – 70.0 µM	0.12 µM	Yousefi et al.,**2018**
Daclatasvir	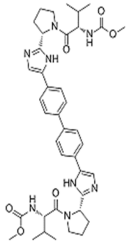	Ni-NPs/MWCNT/GCE	CV, DPV	Tablet and human serum	0.024 – 300 µM	15.8 nM	Joghani et al., **2020**
		AgNPs/GO/CPE	DPV	Pharmaceutical formulation and human urine	25.0 – 12,000 nM	1.6 nM	Azab and Fekry, **2017**
		MnO_2-rGO/CPE	SWV	Human serum and urine	1.0 – 200.0 nM	0.12 nM	El-badawy et al., **2020**
		Pencil graphite electrode	SWV	Plasma	0.20 – 0.70 µM	0.06 µM	Mohamed et al., **2020**
Ledipasvir	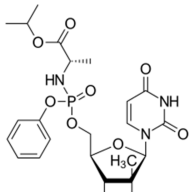	BDDE	CV, SWV	Tablet	0.5 – 60.0 mg L^{-1}	0.12 mg L^{-1}	Allahverdiyeva et al., **2020**
		rGO/NSNiFe_2O_4/MHS	DPV	Tablet and human plasma	0.4 – 350.0 µg L^{-1}	0.1 µg L^{-1}	El-Wekil et al., **2018**
		ε-MnO_2-modified graphite electrode	CV, EIS	Rat plasma samples	0.025 – 3.60 µM	4.5 µg L^{-1}	Abdel-aal et al., **2018**
		GC/(CNT-ILC)/Co	CV	Tablet	0.07 – 1 µM	1.86 nmol L^{-1}	Atta et al., **2019**

Pharmaceutical Compound	Electrode	Method	Medium/Sample	Linear Range	LOD	Reference
	GC/CNT/ILC/rGO/MnO_2	CV, DPV	Human serum	0.0070 – 15 µmol dm^{-3}	0.1 nmol dm^{-3}	Atta et al., **2019**
Valacyclovir 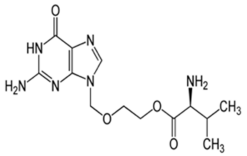	CPE	CV	Urine samples		28.0 nM	Devarushi et al., **2018**
	GCE	DPV	Urine	75.0 – 5,000.0 µM	1.4 µM,	Umesh S. Devarushi, **2013**
	rGO/CPE	CV, SWV	Pharmaceutical and urine samples	10.0 – 50,000.0 nM	1.1 nM	Todakar et al., **2019**
	CPE	CV, SWV	Pharmaceutical and urine samples	50 – 800 nM	1.1 nM	Devarushi et al., **2018**
	SWCNT/GCE	DPV	Pharmaceutical and blood plasma	5 – 55 nM	1.8 nM	Shah et al., **2013**
Acyclovir 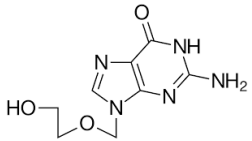	CNT/GCE	CV, LSV, EIS	Tablet	0.08 – 10 µM	30.0 nM	Wang et al., **2006**
	SAM/Au	CV, SWV	Urine	0.01 – 1 µM	10.0 nM	Joseph and Kumar, **2011**
	Cu NPs/CPE	CV, Amperometry	Tablet	27.0 – 520.0 µM	2.6 µM	Heli et al.,**2010**
	PVP/CPE	CV, DPV	Tablet, urine, and human plasma	10 – 750 nM	2.5 nM	Wang et al., **2013**
Flutamide 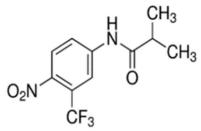	g-C_3N_4/GCE	CV, DPV	Water samples	2.0 – 1208.0 µM	50.0 nM	Kesavan and Chen, **2020**
	GO/GCE	CV, LSV	Human serum	0.009 – 1.9 mM	6.0 nM	R. Karthik et al., **2017a**
	Au electrode	CV, DPV	0.1 M PBS	100.0 – 600.0 µM	1.8 µM	Mehrabi et al., **2019**
	Nano - Ag/MGCE	DPV	Pharmaceutical and urine samples	10.0 – 1000.0 µM	9.3 µM	Ahmadi et al., **2015**
	Boron-doped carbon electrode	SWV	Pharmaceutical, blood, and urine samples	0.9 – 42.9 mM	0.2 mM	Švorc et al., **2017**
Nilutamide 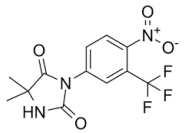	MWCNT/GCE	DPV	Tablet and urine samples	28.0 – 535.0 µM	1.8 nM	R. Karthik et al., **2017b**
	β-CD-AuNP/GO/SPCE	DPV	Human urine samples	0.01 – 193 µM	0.4 nM	Raj Karthik et al., **2017**
	CeV/CNF/GCE	DPV	Human urine	0.01 – 540 µM	2.0 nM	Kokulnathan et al., **2019a**
	SWNPs/SPCE	DPV	Tablet and urine	0.05 – 318 µM	2.6 nM	Sundaresan et al., **2020**
	(MWCNTsf–NGr/CTS)-Cu	DPV	Tablet and blood serum	0.005 − 20 µM	1.6 nM	Akhter et al., **2020**
Taxol 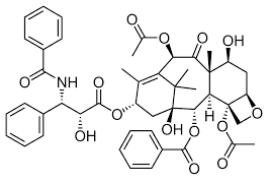	Pencil Graphite	DPV	Plasma	0.70 – 3.0 µM	2.46 nM	Gowda and Nandibewoor, **2014a**
	GCE	LSASV	Urine	1.0 –10.0 µM	12.3 nM	Gowda and Nandibewoor, **2014b**
	Hemoglobin immobilized on the DDAB/SWNTs/Gold electrode	LSASV	0.1 M PBS (pH 7)	14.0 – 100.0 µM	2.8 µM	Zhang et al., **2006**
	DNA immobilization onto the azide-terminated monolayer/Au electrode	DPV	10 mM Tris–HCl buffer solution (pH 7.4)	0.12 – 1.5 µM	12.0 nM	Mehdinia et al., **2008**

Pharmaceutical Compound	Electrode	Method	Medium/Sample	Linear Range	LOD	Reference
	Pencil graphite	DPV	Tablet	0.2 –1.0 µM	80.0 nM	Tajik et al., **2015**

Abbreviations: **ABS**: acetate buffer solution; **Au-In_2O_3-CS/ABPE**: Au-In_2O_3-chitosan modified acetylene black paste electrode; **AuNPs/POM/rGO/GCE**: Au nanoparticles/polyoxometalate/reduced graphene oxide nanohybrid; **BDDE**: Boron-doped diamond electrode; **CB/DPH/GCE**: Carbon black/dihexadecylphosphate film/glassy carbon electrode; **CD-PS**: cyclodextrin-based potentiometric sensor; **CNT**: carbon nanotube; **CNT/Fe_3O_4@PPy/Pd**: Carbon nanotube/Iron oxide polypyrrole nanocomposite; **Co-MOF-on-TPN-COF**: Cobalt-based metal-organic frame work and terephthalonitrile-based covalent organic framework platform; **CPE**: Carbon paste electrode; **ErGO**: Electrochemically reduced graphene oxide; **g-C_3N_4** : Graphitic-carbon nitride; **GCE**: Glassy carbon electrode; **GO**: Graphene oxide; **IL**: Ionic liquid; **MGCE**: Modified (with p-*tert*-butylcalix arene and p-*tert*-butylcalix arene); **mMip- GOX-STR**: redox active magnetic molecularly imprinted polymer-glucose-oxidase-labelled streptomycin; MWCNT: Multiwall carbon nanotube; (MWCNTf–NGr/CTS)-Cu: Multiwall carbon nanotube nitrogen doped graphene and chitosan with electrodeposited copper; **Ni/CR/CPE**: Nickel-curcumin/ carbon paste electrode; **P(L-ASP)/GCE** :Poly(L-Aspartic Acid) modified glassy carbon; **PANI-NF/GCE**: Polyaniline nanofiber modified glassy carbon electrode; **PDDA-Gr/PdNPs**: poly (diallyldimethylammonium chloride) functionalized graphene/palladium nanoparticles; **QDs-P6LC-PEDOT:PSS/GCE**: Printex 6L carbon and cadmium telluride quantum dots within a poly(3,4-ethylenedioxythiophene)polystyrene sulfonate film; **rGO**: reduced graphene oxide; **rGO/NSNiFe_2O_4/MHS**: 3D $NiFe_2O_4$ nanospheres and reduced graphene oxide supported by morpholinium acid sulphate; **SPCE**: Screen printed carbon electrode; **SPGE**: Screen-printed graphite electrode; **SWCNT**: Single-walled carbon nanotube; **SWNP**: $Sm_2(WO_4)_3$ nanoparticles; **TRSiN/GCE**: three-dimensional redox active organosilica nanostructure.

Highlights

- Different electroanalytical techniques used for electrochemical sensing;
- Rationale design of nanomaterials for the development of electrochemical sensor;
- Recent advances in electrochemical detection of pharmaceutical drugs;
- Opportunities and challenges of developing high-performance electrochemical sensors;
- Applications of electrochemical sensor in medicine and environment.

Declaration of interests

☒ The authors declare that they have no known competing financial interests or personal relationships that could have appeared to influence the work reported in this paper.

☐The authors declare the following financial interests/personal relationships which may be considered as potential competing interests: